

NEUTRON FLUX MEASUREMENT BY ACTIVATION METHOD AND
STUDY OF NEUTRONS AND GAMMA RAYS ATTENUATION
PROPERTIES OF MULTILAYERED SHIELDS

by

MD. ABDUL MATIN

Submitted in Partial Fulfilment of the
Requirements for the
Degree of M. Phil



Department of Physics
Bangladesh University of Engineering and Technology

August 1990



BANGLADESH UNIVERSITY OF ENGINEERING AND TECHNOLOGY, DHAKA, BANGLADESH
DEPARTMENT OF PHYSICS
CERTIFICATION OF THESIS WORK
A THESIS ON

"NEUTRON FLUX MEASUREMENT BY ACTIVATION METHOD AND
STUDY OF NEUTRONS AND GAMMA RAYS ATTENUATION
PROPERTIES OF MULTILAYERED SHIELDS"

BY

MD. ABDUL MATIN

has been accepted as satisfactory in partial fulfilment of the Degree of Master of Philosophy in Physics and certify that the student demonstrated a satisfactory knowledge of the field covered by this thesis in an oral examination held on 10th October, 1990.

Board of Examiners

1. Prof. Gias Uddin Ahmad
Head, Dept. of Physics, BUET.

Prof. Gias Uddin Ahmad 20-10-90
Supervisor and Chairman

2. Dr. M. Azizur Rahman
Head, Reactor and Neutron
Physics Division, INST.,
BAEC, Savar.

Dr. M. Azizur Rahman
Co-Supervisor and Member

3. Prof. M. Ali Asgar
Dept. of Physics, BUET.

Prof. M. Ali Asgar
Member 20/10/90

4. Dr. Mominul Haq
Dept. of Physics, BUET.

Dr. Mominul Haq 20/10/90
Member

5. Prof. H.M. Sengupta
Dept. of Physics,
Dhaka University, Dhaka.

Prof. H.M. Sengupta 20/10/90
Member (External)

539.215
1970
ABD

C E R T I F I C A T E

This is to certify that the author is solely responsible for the work reported in this thesis and that this work has not been submitted to any university or elsewhere for the award of a degree/diploma.

Md. Abdul Matin *98/22, 22/22*

(MD. ABDUL MATIN)
Candidate

98/22, 22/22
(DR. M. AZIZUR RAHMAN)

Co-Supervisor
Head, Reactor and
Neutron Physics Division,
INST, Savar and
Chief scientific Officer
BAEC

98/22, 22/22

(DR. GIAS UDDIN AHMAD)
Supervisor
Professor of Physics
BUET

ACKNOWLEDGEMENT

The author expresses his profound gratitude to his supervisors Prof. Gias Uddin Ahmad, Department of Physics, Bangladesh University of Engineering and Technology (BUET) and Dr. M. Azizur Rahman, Head, Reactor and Neutron Physics Division, Institute of Nuclear Science and Technology (INST), Bangladesh Atomic Energy Commission (BAEC), Savar, for their constant guidance and supervision throughout the progress of this work.

The author is grateful to Dr. Farid Uddin Ahmed, Senior Scientific Officer and Mr. A.S. Mollah, Senior Scientific Officer, both of INST, Savar, for their encouragement and many valuable suggestions.

The author takes this opportunity in extending his gratitude to all members of Reactor and Neutron Physics Division (INST) and particularly to Mr. M. Ahad Ali, S.A.-I, for their untiring help and co-operation.

The author would like to thank gratefully Mr. A. Hye Chowdhury, Lecturer, Department of Physics, BUET and a fellow research worker for his constant help, encouragement and many useful discussions.

The author expresses his sincere gratitude to Prof. M.A. Asgar and Prof. T. Hossain and others of the Department of Physics (BUET), for their encouragement and keen interest.

The author is grateful to Dr. M.A. Mannan, Chairman and Dr. S.M.M.R. Chowdhury, Member, Physical Science, BAEC and Dr. M. Serajul Islam, Director General, Atomic Energy Research Establishment (AERE), BAEC, Savar, for their encouragement and interest.

The author expresses his gratitude to BUET and to BAEC for extending financial assistance and technical and laboratory facilities during the course of this work.

Finally, the author would like to express his deep gratitude to his wife Mrs. Shahinur Begum for her continued help, encouragement and understanding throughout the progress of this work without which this thesis would not have been possible.

A B S T R A C T

The neutron flux distribution at various distances from the biological shielding face of the tangential beam port of the TRIGA Mark-II 3 MW Research Reactor has been measured by activation technique for neutron radiography set up. In order to determine suitable material for shielding of personnel and equipments, the gamma and neutron attenuation properties of multilayered shields, composed of different materials, were studied by using a californium-252 source. Californium-252 emits both gamma rays and neutrons and the emission characteristic is similar to that inside a reactor core. It was found that a multilayered shield of polyboron-heavy concrete possesses the best possible attenuating properties for neutron. While a similar shield but composed of polyboron-lead was found to possess the best possible attenuating properties for gamma-rays.

C O N T E N T S

			<u>PAGE</u>
CHAPTER-1	NEUTRON FLUX MEASUREMENT BY ACTIVATION METHOD.		
1.1	INTRODUCTION	...	1
1.2	EXPERIMENTAL PROCEDURE	...	2
1.2.1	HIGH PURITY GERMANIUM DETECTOR	...	2
1.2.2	HIGH VOLTAGE SUPPLY (E.H.T. SUPPLY)	...	7
1.2.3	PRE-AMPLIFIER	...	9
1.2.4	SPECTROSCOPY AMPLIFIER	...	9
1.2.5	MULTICHANNEL ANALYZER	...	10
1.2.6	INTERACTION OF GAMMA-RAY WITH HPGe DETECTOR	...	11
CHAPTER-2			
	ENERGY RESOLUTION OF THE HPGe DETECTOR	...	14
2.1	THE DETECTOR CONTRIBUTION	...	15
2.2	THE ELECTRONIC CONTRIBUTION	...	16
2.3	TOTAL SYSTEM PERFORMANCE	...	16
2.4	EFFICIENCY MEASUREMENTS OF HPGe DETECTOR	...	17
2.4.1	PROCEDURE	...	20
2.4.2	IRRADIATION SETUP	...	24
2.4.3	CALCULATION OF NEUTRON FLUX	...	25
CHAPTER-3			
	RESULTS AND DISCUSSION	...	29

			<u>PAGE</u>
CHAPTER-4	STUDY OF NEUTRONS AND GAMMA RAYS ATTENUATION PROPERTIES OF MULTILAYERED SHIELDS		
4.1	INTRODUCTION	...	30
4.2	REVIEW OF EARLIER WORKS	...	31
4.3	INTERACTION OF NEUTRONS WITH MATTER	...	34
4.4	INTERACTION OF GAMMA-RAYS WITH MATTER	...	37
4.5	DEFINITION OF SOME NUCLEAR PROPERTIES	...	37
CHAPTER-5	EXPERIMENTAL METHOD		
5.1	EXPERIMENTAL SETUP	...	45
5.2	NEUTRON DETECTOR	...	52
5.3	GAMMA-RAY DETECTOR	...	62
5.4	RADIATION SOURCE	...	70
5.5	SHIELDING MATERIALS	...	74
CHAPTER-6	RESULTS AND DISCUSSION	...	79
CHAPTER-7	CONCLUSION	...	88
	REFERENCES	...	90

CHAPTER-1

NEUTRON FLUX MEASUREMENT BY ACTIVATION METHOD



1.1 INTRODUCTION

There are a number of facilities to carry out experiments with neutrons from the TRIGA Mark-II JMW(t) research reactor at the Atomic Energy Research Establishment (AERE), Savar, Dhaka. This reactor has four beam ports, out of which two are radial beam ports, one is piercing beam port and the other is a tangential one. Gamma-ray background is least in the tangential beam port. The knowledge of neutron flux at different distances from the biological shielding face along the central line of the tangential beam port of the reactor is essential for proper planning of the neutron radiography experiments and the meaningful interpretation of their results. Hence it is necessary to find out the neutron flux at the point of interest in the neutron radiography experiment facilities of the tangential beam port of the reactor.

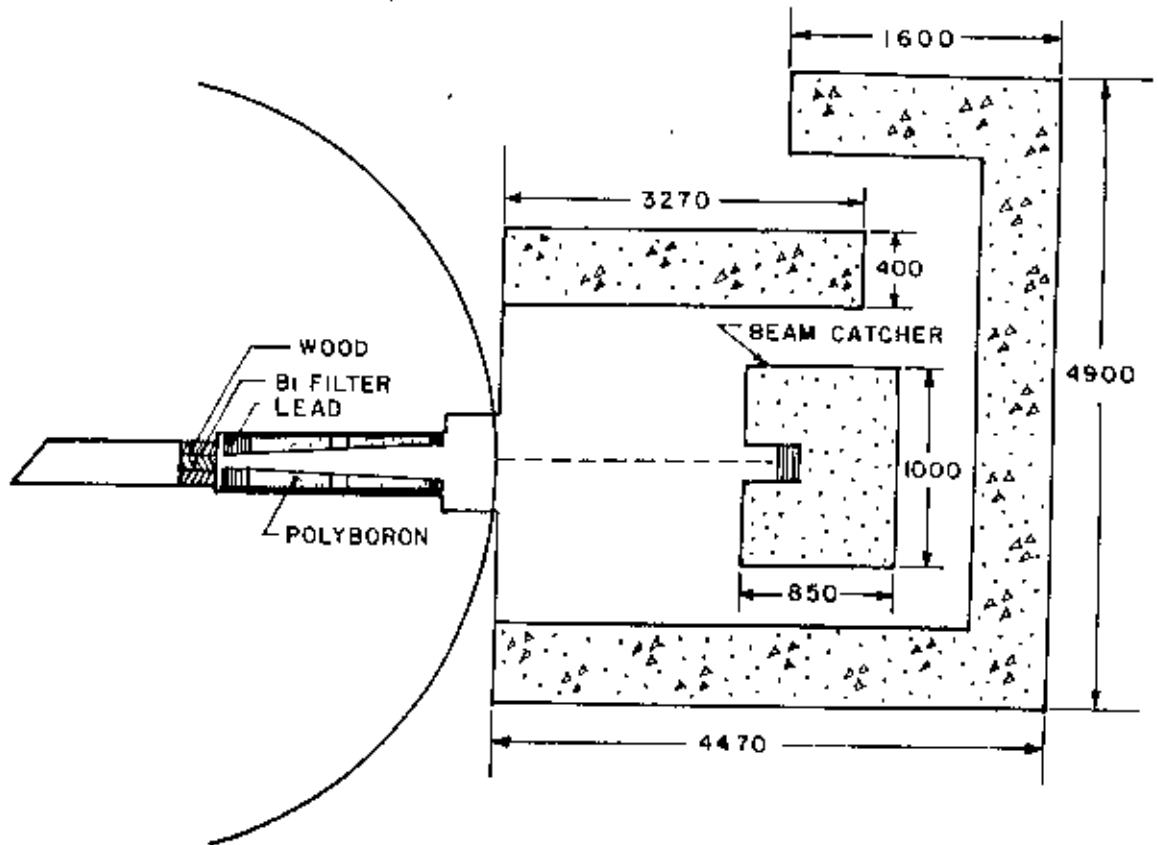
The measurement of neutron flux is commonly carried out by the activation technique. In this technique, gold foils (^{197}Au) of different masses are irradiated to the neutron beam. The foils become radioactive as a result of the neutron irradiation. The activity induced in a foil is dependent on the amount of target element present, activation cross-section of the reaction of interest, the irradiation flux, the duration of irradiation and the decay characteristics of the radionuclide formed. The activity of the radioactive products produced is measured by a high purity germanium (HPGe) detector. Normally gamma-rays emitted by the irradiated sources are of low intensity. Hence the efficiency of the detector for counting this low-intensity γ -rays should be accurately known so that from a knowledge of the relevant cross-section producing a particular isotope emitting a characteristic γ -ray, the neutron flux can be determined.

1.2 EXPERIMENTAL PROCEDURE

The block diagrams of the experimental set-up for irradiation of gold foils at the tangential beam port (the gold foil was placed at different distances) of the TRIGA Mark-II 3MW(t) research reactor at the AERE, Savar and the counting system are shown in figures 1 and 2, respectively. When an ionizing radiation passes through the detector it loses energy by ionizing collision in the sensitive region of the detector and produces electron-hole pair in the semi-conductor detector. When an external electric field is applied to this detector the charge carriers move towards the respective polarity of the electric field. These are collected and subsequently converted into a voltage pulse using a preamplifier. The signal from the preamplifier is amplified by an amplifier and the output is analyzed by the multichannel analyzer (MCA). Finally a printer was used to print out the data collected in MCA. A brief description of the semi-conductor detector and various electronic equipments used are given below.

1.2.1 HIGH PURITY GERMANIUM (HPGe) DETECTOR

For the detection of gamma-ray emitted by the radioactive sources and reaction products a HPGe detector⁽¹⁾ was used. HPGe detectors are primarily used for high resolution spectroscopy of gamma radiations and occasionally, charged particles. Charged particles lose their energy mainly through the ionization in the sensitive region of the detector. High purity germanium gamma-ray spectrometer is a high quality precision instrument with the best available performance and reliability. The high resolution of the detector makes it possible for more detailed studies of gamma-ray spectra than any other detector.



[ALL DIMENSIONS ARE IN mm]

FIG. 1 BLOCK DIAGRAM OF THE EXPERIMENTAL SETUP FOR IRRADIATION

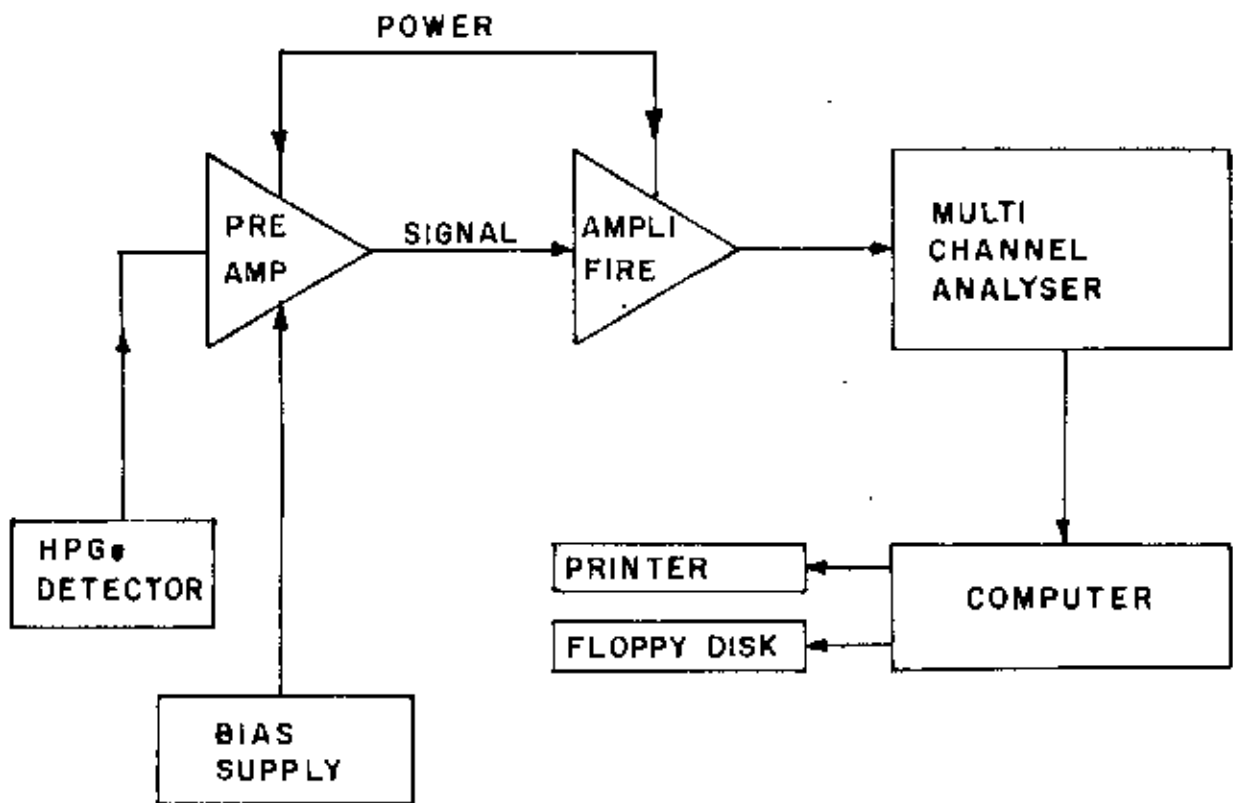


FIG. 2. BLOCK DIAGRAM OF DETECTION SYSTEM.

PHYSICAL PROPERTIES

In Table-1, some of the physical properties of the "intrinsic germanium" or "high purity germanium" are summarized:

TABLE-1

Atomic No.	32
Atomic Wt.	72.60
Density	5.33 gm/cm ³
Atoms	4.41 x 10 ²² /cm ³
Dielectric constant	16
Forbidden energy gap (OK)	0.746 eV
Energy per electron-hole pair (77°K)	2.96 eV
Fano factor (77°K)	0.058 (Ref-2)
Energy gap (77°K)	0.75

A HPGe detector is fabricated from pure germanium crystals and containing an equal number of free charge carriers through out its volume. This is basically a cylindrical germanium crystal with an n-type contact on the outer surface with a high concentration of free electrons and practically no free holes and a p-type contact on the surface of the axial wall with an excess of holes but very few electron. The germanium has a net impurity level of around 10¹⁰ atoms/cm³. The intrinsic region is formed by depletion of charges with the application of reverse bias voltage across the diode, which is sensitive to ionizing radiation, particularly

x- and γ -rays. When photons interact within the depletion region (sensitive region) of a detector, high speed electrons are produced, which lose their energy by creating free charge carriers (electron-hole pair). The pairs are swept out by the electric field to their collecting electrodes where a charge sensitive pre-amplifier converts this charge into a voltage pulse proportional to the energy deposited in the detector.

The electron-hole pair is somewhat analogous to the ion-pair created in the gas-filled detectors. An advantage of HPGe detectors are

- (i) One can avoid lengthy process of lithium drifting.
- (ii) Detector can be kept at room temperature when not in use.

The absorbed charge spectrum consists of a continuum and one or more narrow peaks from which one can deduce the incident gamma-ray flux. In the energy spectrum, the areas under the peaks are a function of the detector size and shape, the position of the source with respect to the detector and the photon energy. However the widths of the peaks and hence the heights relative to the continuum are determined by the energies of the photons, the intrinsic resolution of the detector and the noise contribution of the amplifying and measuring system.

Because germanium has a relatively low ionization energy, these detectors must be cooled in order to reduce the thermal generation of charge carriers to an acceptable level. Otherwise, noise induced by leakage current destroys the energy resolution of the detector. Liquid nitrogen, which has a temperature of 77°K is the common cooling medium for such detectors.

In this study a closed-end-coaxial HPGe detector was used for counting because it presents a uniform cross-section of active detector

volume to radioactive samples that are counted a short distance from the detector. The physical/performance data of HPGe detector which is used in this works are:

Geometry	:	Closed-End-Coaxial
Length	:	55 mm
Diameter	:	41 mm
Active area facing window	:	17.50 cm ²
Distance from window	:	5 mm

ELECTRICAL CHARACTERISTICS (3)

Depletion Voltage	:	+ 3500 Vdc
Recommended Bias Voltage	:	+ 3500 Vdc
Leakage Current at Recommended Bias	:	0.25 Na
Preamplifier Test Voltage at Recon.Bias:	:	0.6 Vdc
Capacitance at Recommended Bias	:	24 Pf.

1.2.2 HIGH-VOLTAGE SUPPLIES (E.H.T. Supply)

All radiation detectors require the application of an external high voltage for their proper operation. This voltage is conventionally called "detector bias" and high voltage supplies used for this purpose are often called detector bias supplies. Some pertinent characteristics of the detector bias supplies are:

- 0 The maximum (and minimum) voltage level and its polarity.
- 0 The maximum current available from the supply.

- 0 The degree of regulation against long-term drifts due to changes in temperature or power line voltage.
- 0 The degree of filtering provided to eliminate ripple at power line frequency or other low-frequency noise.

The sophistication required of the bias supply varies greatly with the detector type. Typical scintillation high-voltage supplies must be capable of providing up to 5000 volts with a current of a few milliamperes. The output must also be well regulated to prevent gain shift in the photomultiplier tube due to drifts in the high voltage level. Bias supplies for proportional counters must also supply relatively high voltages, but the current demands are considerably less. However, the degree of regulation and filtering is again important because any high-voltage fluctuations appear superimposed on the signal. Semiconductor diode detectors draw relatively little current and the voltage demands seldom exceed 1000 volts. Canberra Model 3105 High Voltage Power Supply was used in our experiment. Its salient features⁽⁴⁾ are as follows:

- 0 Regulated 0 to \pm 5000 VDC, 100 μ A output.
- 0 Noise and ripple \leq 30 mV peak to peak.
- 0 Protected against overload and short circuit.

It is designed for operation with a wide variety of detectors. Its noise and ripple characteristics make it suitable for surface barrier detectors, while the 2 mA current capability permits operation with scintillation detector. By design, the 3105 high voltage power supply will accommodate all types of detectors requiring 5 KV or less.

1.2.3 PREAMPLIFIER

The output of the radiation detector appears as a pulse of voltage or charge which is so small that it is impractical to deal with the signal pulses without an amplification step. Therefore, the first element in a signal processing chain is often a preamplifier, provided as an interface between the detector and the pulse processing electronics that follow. From a signal-to-noise standpoint, it is always preferable to minimize the capacitive loading on the detector, and therefore long interconnecting cables between the detector and preamplifier should be avoided as much as possible. The preamplifier should, therefore, be located as close as possible to the detector.

The Canberra Model 2001 represents the latest advance in charge sensitive pre-amplifiers. It was designed primarily for high resolution gamma spectroscopy using cooled Ge solid state detectors. The performance⁽⁵⁾ of the Model 2001 is the current state of the art for room temperature (non-cooled) pre-amps. The noise level for the 2001 is equivalent to less than 600 eV with a negligible source capacitance. The pulse decays exponentially with a time constant of 50 μ sec. Power for the Model 2001 is usually supplied from the associated pulse shaping amplifier.

1.2.4 SPECTROSCOPY AMPLIFIER

The major role of an amplifier is to convert the preamplifier output signal into a form most suitable for the desired measurement. The Canberra Model 2021 Spectroscopy Amplifier offers the modern spectroscopist

more performance, features and flexibility than any other nuclear pulse amplifier available today. The Model 2021's exceptional DC stability and ultra low noise make certain that optimum performance is realised. The Model has a d.c. input impedance of approximately 1000 Ω and accepts either positive or negative pulses from the preamplifier. This unipolar output is used for spectroscopy when d.c. coupling can be maintained from the 2021 amplifier to the analyzer. The unipolar output can be selected for either positive or negative polarity.

1.2.5 MULTICHANNEL ANALYZER (MCA)

The operation of the multichannel analyzer is based on the principle of converting an analog signal (the pulse amplitude) to an equivalent digital number. The basic function of the MCA involves only the ADC (analog-to-digital) and the memory store and a display.

Particles penetrating the depletion region in the detector, give rise to pulses whose amplitudes correspond to the loss of energy of the particle. The pulses are then digitized by ADC and the output of the ADC is stored in a computer type memory, which has as many addressable locations as the maximum number of channels into which the recorded spectrum can be subdivided. The channel number is the memory address and is proportional to the input signal voltage. Each pulse is digitized and counts are added to the appropriate memory location, so that a spectrum of number of pulses vs. voltage is obtained. Once the data is stored, it can be displayed through various systems, namely on a cathode ray oscilloscope, pen recorder or through a teletype writer and cassette recorder.

The Canberra series 35 MCA⁽⁶⁾ is a versatile system in many ways. The spectrum can be recorded over 4096 channels or in any of the subgroup.

1.2.6 INTERACTION OF GAMMA-RAYS WITH THE HPGe DETECTOR

The measured features of the differential pulse-height spectrum are directly related to the three primary processes in which incident gamma-ray photons give up all or part of their energy in single events. They are: photo-electric effect, Compton scattering and pair production. Contributions to the full energy peak may also arise from photo-electric encounters by the gamma-rays following one or more Compton scattering within the detector.

PHOTOELECTRIC EFFECT

In a photo-electric encounter the entire photon energy is absorbed by a bound atomic electron and appears as (i) the K.E. of that electron as it is ejected and (ii) an x-ray or Auger electron emitted by the residual ion. The cross-section for the photo-electric process is proportional to Z^5 and increases rapidly with decreasing photon energy. The low energy x-ray is almost invariably absorbed in a second photo-electric event before it can escape from the crystal. As a result, the photon energy appears as electron kinetic energy. For the photo-electric effect, a monoenergetic gamma-ray thus gives rise to a mono-energetic peak in the charge distribution corresponding to the incident photon energy, E.

COMPTON SCATTERING

In this process the photon is scattered by an electron with a partial energy loss depending on the angle of scattering. The electron kinetic energy lies between zero and an upper energy limit which depends on the photon energy. Between these limits, the scattering gives rise to a continuous electron-energy distribution, i.e., the Compton continuum. The cross-section for this process is not as highly energy dependent as the photo-electric effect and is proportional to the Z of the scattering materials.

PAIR PRODUCTION

Pair production has an energetic threshold equal to the combined positron-electron rest mass (1.022 MeV). The cross-section increases rapidly above this threshold and is proportional to the Z^2 of the scattering material. The entire photon energy is absorbed and appears as the total K.E. of the positron-electron pair ($E-1.022$ MeV) plus the rest mass of the pair. The positron is unstable and will annihilate with an atomic electron, usually when it has come to rest.

In such a case the annihilation produces two photons of energy 0.511 MeV each emitted at 180° to each other. In the usual encounter, both annihilation photons will escape. Then a mono-energetic gamma-ray gives rise to a electron distribution of energy $E-1.022$ MeV. Satellite peaks may appear if the detector is sufficiently large. These correspond to the absorption of one or both annihilation photons in photo-electric encounter. Ultimately three peaks are seen one at $E-1.022$ MeV, corresponding to the

escape of both photons (e-escape), one at $E-0.511$ MeV, corresponding to the escape of one photon (1-escape) and one at E (full-energy peak) corresponding to the escape of neither photon.

CHAPTER--2

ENERGY RESOLUTION OF HPGe DETECTOR

The dominant characteristic of germanium detectors is their excellent energy resolution when applied to gamma ray spectroscopy. The great superiority of the high purity germanium (HPGe) detector system in energy resolution allows the separation of closely spaced gamma-ray energies, which remain unresolved in the NaI(Tl) spectrum. Consequently, virtually all gamma ray spectroscopy that involves complex energy spectra has been carried out with germanium detectors.

The overall energy resolution achieved in a HPGe detector system is normally determined by a combination of two factors:

- (i) Contributions from the HPGe crystal and
- (ii) Contributions of electronic noise.

These two factors are dependent on the energy of the radiation and the inherent quality of the detector in use. The full width at half maximum W_t of a typical peak in the spectrum due to the detection of a monoenergetic gamma ray can be synthesized as follows:

$$W_t^2 = W_D^2 + W_e^2$$

where the W values on the right-hand side are the peak widths that would be observed due only to effects of carrier statistics and electronic noise.

2.1 THE DETECTOR CONTRIBUTION

When gamma rays interact with the crystal of the HPGe detector high speed electrons are produced. These high speed electrons loses energy in passing through matter, occuring in both ionizing and non-ionizing collisions. The average energy loss per ionizing collision is about 2.96 ev/ (electron-hole pair) in germanium. Thus, there will be on the average, approximately 3.38×10^5 pairs formed in stopping a one MeV electron. Due to the statistical behaviour of the production of electron-hole pairs, there are fluctuations in the actual number of carriers which are produced. The statistical behaviour is not an uncorrelated one, however, and the variance is considerably smaller than would be deducted from poisson statistics. Neglecting the small effect of the statistical fluctuations, the detector contribution to the energy resolution for germanium, is

$$\text{Detector FWHM, } W_D^2 = (2.35)^2 F_F E (\text{KeV})$$

where

F : Fano factor, $F_{\text{Lowest}} = 0.058$ (Ref.2)

ϵ : Average energy necessary to create one electron-hole pair, and

E : Gamma ray energy in MeV.

In addition to the inherent resolution, there will also be a spread due to incomplete charge collection and leakage current. Incomplete charge collection gives rise to an asymmetric photo-peak with a tail on the low energy side.

2.2 THE ELECTRONIC CONTRIBUTION

The electronic system consists primarily of three parts: the preamplifier, the spectroscopy amplifier, and the multichannel analyser. Each may contribute to the resolution width, but with proper adjustments, the noise contribution of the electronic system is limited to that of the preamplifier. The typical low noise charge sensitive FET preamplifier can be characterized by two parameters: the noise output with zero capacitance and the slope of the noise vs. input capacitance. The input capacitance arises from both the inherent detector capacitance and from the connecting cable between the detector and the preamplifier. It is therefore important to keep the interconnecting cable as short as possible, and to choose a detector whose inherent capacitance is no larger than necessary. Each connector adds about 2 or 3 pF, and typical co-axial cables may add from 15 to 30 pF/ft. These considerations are most important when observing low energy gamma-rays, because the statistical contribution to the noise is small and the preamplifier noise dominates.

2.3 TOTAL SYSTEM PERFORMANCE

At energies of a few hundred keV or less, the system resolution is dominated by the pre-amplifier. A specially constructed cryogenically cooled FET pre-amplifier detector system should be used to take advantage of the resolution capability of HPCe detectors at low energies. The energy resolution is primarily determined by the width of the peak and

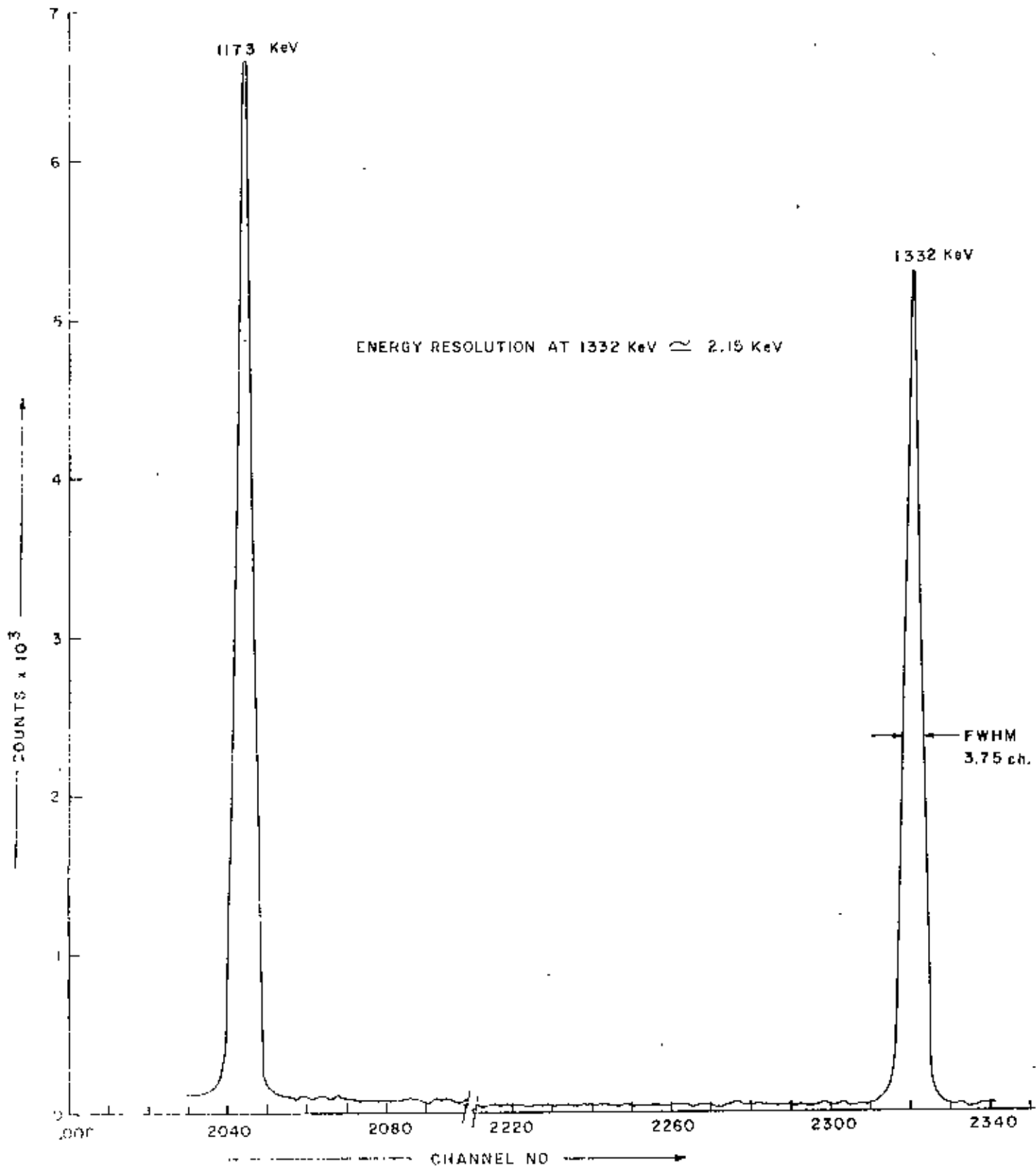


FIG 3

arises from the statistical variation in the pulse heights as recorded from nominally monoenergetic particles. In this work the gamma-ray spectrum with ^{60}Co standard source of known strength was taken to obtain the detector resolution. The full width at half maximum (FWHM) is 3.75 channel and the energy per channel is 0.574 keV at 1332 keV as shown in fig. 3 . The detector resolution (FWHM) is 2.15 keV.

2.4 EFFICIENCY MEASUREMENTS OF HPGe DETECTOR

Emission rate measurement for gamma radiation by means of germanium semi-conductor detectors have become a routine procedure in many fields of fundamental and applied research. If accurate emission rates are needed, a reliable efficiency calibration of the detector has to be carried out. For that purpose most laboratories use standard sources of known strength. Various gamma spectrometer are widely used for gamma-ray spectroscopic measurements. In the past, NaI(Tl) spectrometers were exclusively used for the estimation of gamma activities in different radioactive samples. However, their poor resolution often resulted in time consuming and tedious measurements. At present high sensitivity gamma-ray spectrometers HPGe are widely used for direct analysis of radioactive samples. Their high energy resolutions have greatly enhanced the differentiation of individual emitters from a complex mixture of radionuclides present in a sample. Great care must be exercised in calibrating the efficiency because the over all uncertainty of the measurement will be limited by the uncertainty of the efficiency value. The efficiency calibration is normally carried out for an assortment of gamma-ray energies covering the range of interest to allow

construction of an empirical efficiency versus energy curve. Most of the gamma-ray emitted by the nuclides to be studied here had energies between 50 KeV to 1800 KeV.

One should consider several points before undertaking the actual determination of efficiency

- (i) Sample counting configuration
- (ii) Calibration of sources
- (iii) Calibration methods.

The most common approach to calibration of Ge detectors is the experimental determination of Full Energy Peak efficiency as a function of energy for each counting configuration. The counting efficiency at any particular gamma-ray energy is dependent on a number of factors. Most of these are associated with the photon interaction process within the detector, the source-detector geometry or with gamma-ray attenuations within the source or from surrounding materials. In the present work, calibration⁽⁷⁾ was carried out for gamma-ray energy between 81-1332 keV in a specific geometry.

The efficiency calibration is easy if the sample to be measured and the calibration source contain the same radionuclides. However, if the sample emits photons of an energy different from that of the calibration source photons, the efficiency for the energy of interest has to be interpolated between two or more calibration points. The efficiency of the detector is mainly dependant on the energy of radiation and source-to-detector geometry. In gamma-ray spectroscopy, it is essential to obtain

the absolute yield from the observed gamma-ray spectra. This can be achieved only if the efficiency of the detector is known.

The efficiency is defined as the number of events counted in a peak in a gamma-ray spectrum divided by the number of events actually produced by the mono-energetic source over 4 π geometry and the efficiency is quoted in per centage. The photo-peak detection efficiency of the HPGe detector was determined in this work as follows: From the measured spectra, the peak areas of the selected gamma-ray lines were determined by direct summation of the channel counts, which automatically subtracts the corresponding background counts. The background count is assumed to be linear. The counts rates were obtained from the net area of the peaks.

The full energy peak efficiency ϵ for the photon energies E of different radioactive sources and targets was determined using the relation:

$$\text{Efficiency, } (\%) = \frac{\text{Counts/sec.}}{\text{activity} \times I_{\gamma}(\%) } \times 100$$

The activity was calculated from the relation

$$\text{Activity, } A = A_0 e^{-\lambda t}$$

The factor $\exp(-\lambda t)$ was calculated from the half-lives of the sources. The calculations are shown in Table-2.

2.4.1 PROCEDURE

The radioactive sources of known strength used for the calculation of the detector efficiency are Na-22, Mn-54, Co-60, Co-57, Ba-133 and Cs-137 were supplied by the Institute of Nuclear Science and Technology (INST) at Savar, Bangladesh. The experimental setup for the detector efficiency consists of radioactive sources and a detection system. The counting was done by placing the source directly on the middle of the surface of the detector and the angle between the source and detector was 0° . The source and the detector were placed within the lead shielding. The interaction of gamma-ray with the system takes place in the detector. The output signal of HPGe detector obtained from the preamplifier was fed into an spectroscopy amplifier (Model 2021). These amplified pulses were then analysed by a Canberra Model 4096 MCA series 35. The efficiency measurement was done with simplest, most straight forward MCA settings so as to minimize the ADC dead time and effort required to integrate the peaks. For these reasons, we use the 1024 channel range and memory size with no digital offset.

When efficiency data have been taken for a sufficient number of energies in the energy region of interest, a graph is plotted for the efficiency - versus - energy. The decrease in efficiency shown at low energies is caused by absorption of photons by sample matrix, cryostat end cap, and dead layer of the detector itself. The gradual decrease in efficiency at higher energies occurs because of the reduction in the cross-section for interaction of the detector material (i.e., Ge)

with increasing energy of the incident photon. For low energy γ -rays (below 2 MeV), the FEP is relatively intense and is essentially Gaussian in shape. The curve is shown in fig.4.

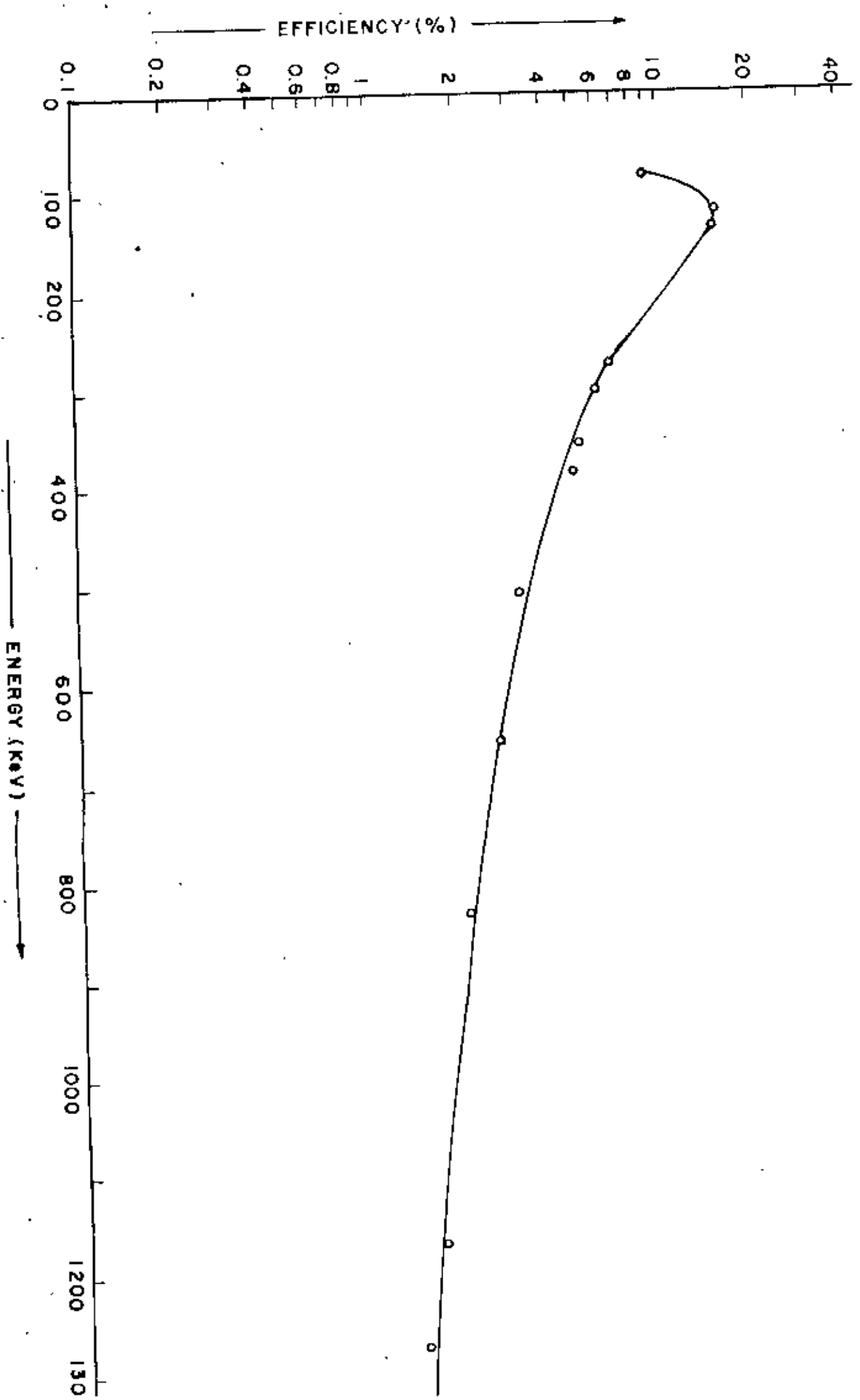


FIG. 4

Table-2

Source	E_γ (keV)	Isotopic abundance (%) I_γ	Half-life ($t_{1/2}$) in days	Source strength, A_0 in Bq(dps)	$e^{-\lambda t}$	Activity $\times 10^4$ Bq	Efficiency (%)
^{60}Co	1332	99.98	1925.38	37259	0.89	3.34	1.38
	1173	99.87		04-01-88			2.22
^{57}Co	136	10.58	271.65	232693	0.03	0.79	15.61
	122	85.59		16-03-85			15.75
^{54}Mn	835	99.97	312.20	208791 27-03-85	0.05	1.13	
^{137}Cs	662	85.1	11013.51	33411 04-01-88	0.98	3.28	3.05
^{22}Na	1274	99.94	949.73	133496	0.38	5.12	1.22
	511	180.8		28-03-85			3.15
^{133}Ba	81/82	32.5	3832.50	103008 26-03-85	0.79	8.12	87.62
	276	7.03					6.47
	303	18.6					6.14
	356	61.6					5.23
	384	8.88					5.14

2.4.2 IRRADIATION SETUP

The irradiation setup used is shown in fig.1. Out of the four beam ports of the 3MW(t) TRIGA Mark-II research reactor, AERE, Savar, the tangential beam port (TBP) has been chosen for the irradiation work, because of low gamma background. To reduce the gamma radiation background around the irradiation facility of the TBP of the reactor, a biological shielding house has been constructed. The neutrons are produced by fission in the reactor core which come out through the TBP. In order to have a collimated neutron beam from the TBP of the reactor a 120 cm long conically shaped aluminium hollow cylinder having a 5 cm diameter at the inner end and 10 cm diameter at the outer end was made. This conical cylinder was then inserted inside another hollow aluminium cylinder of 20 cm uniform diameter of the same length and fixed together with flanges at both ends. The empty space between the two cylinders was fitted up with paraffin wax and boric acid in the ratio 3:1 by weight. Three lead rings (15 cm in the front, 10 cm in the middle and 1.5 cm in shielded face of the reactor) were also put in the inner side of the collimator for gamma shielding.

In order to measure the neutron flux distribution at different distances from the tangential beam port of the reactor the samples were placed in the neutron beam for a specified time. The high purity gold foils (100% abundance) having different masses (60, 62.9, 59.6 and 58.9 mg) were used for irradiation. The foil was attached first on the aluminium strip by scotch tape and it was then suspended in such a way that the foil just lies on the central line from outside of the biological shielding face of the beam port of the reactor. The foils, placed at 0, 50, 100 and 140 cm

from the shielding face along the central line of the tangential beam port weighed 60, 62.9, 59.6 and 58.9 mgm respectively. The time of irradiation in each case was one hour. At the end of irradiation time, the foil was removed from the reactor and a cooling period was allowed before the induced radioactivity were measured by a co-axial HPGe detector under the identical condition that was used for efficiency calibration of the HPGe detector. The measured radiation was then used to deduce information about the number and energy distribution of the neutron in the original field. The most widely used reaction in activation technique is called the radiative capture of the (n, γ) type. The reaction in the present work is $^{197}\text{Au}(n, \gamma)^{198}\text{Au}$.

DATA

DET-1

Reactor power	:	400 KW
Half-life of ^{198}Au	:	2.695 days
Decay constant of the product nucleus	:	$1.78 \times 10^{-4} \text{ min}^{-1}$
Gamma-ray energy	:	411 keV
Efficiency of the detector at 411 keV	:	5.1%
Average cross-section for ^{197}Au	:	98 b

2.4.3 CALCULATION OF NEUTRON FLUX

The basic equation of the neutron activation technique is given by

$$A_0 = n\sigma\phi(1 - e^{-\lambda t_i}) \quad \dots \quad (2a)$$

where,

- A_0 : activity at the end of the irradiation
 n : total number of target nuclei
 σ : the activation cross-section in barns
 ϕ : the neutron flux
 t_i : the time of irradiation
 λ : the decay constant of the product nucleus
 $(1-e^{-\lambda t_i})$: saturation factor depending upon the irradiation time ' t_i ' and the half-life of the radionuclides formed.

Therefore, the neutron flux can be calculated from the measured value of the initial activity A_0 , the irradiation time t_i , the decay time t_d , weight w , and the known value of nuclear data such as half-life and cross-section.

The neutron flux were calculated from the expression (2a). However, the count rates at end of the irradiations were subjected to usual corrections for the photpeak detection efficiency ϵ . The data for this correction was taken from the literature. Thus the expression for ϕ , $n/\text{cm}^2\text{-sec}$, can be obtained as follows applying the usual correction. The total disintegration/sec. is

$$A = \frac{\text{Counts/sec}}{\epsilon(\%) \times I_{\gamma}(\%)}} \dots \quad (2b)$$

where,

I_{γ} = isotopic percentage composition(%)

The total number of nuclei

$$n = \frac{\text{Weight (W)} \times \text{Avogadro's no. (N)}}{\text{Atomic weight}}$$

Therefore,

$$\phi = \frac{A e^{-\lambda t_d}}{n \sigma (1 - e^{-\lambda t_d})}$$

where t_d = decay time

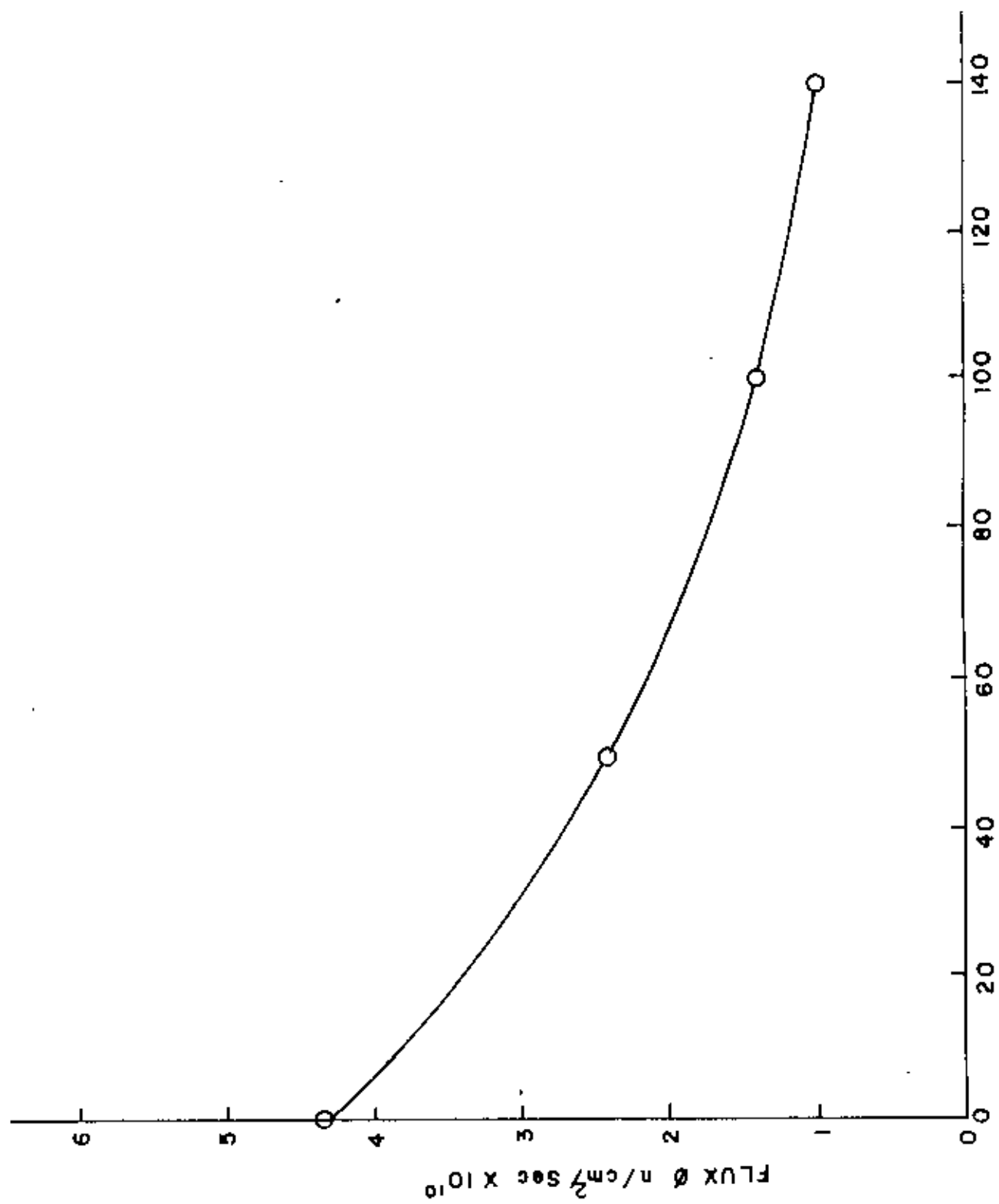
The neutron flux as calculated by equation 2c was found to be of the order of $4.388 \times 10^7 - 1.085 \times 10^7$ n/cm²/sec and is shown in Table-3. Efficiency of the detector had been measured earlier. The curve(5) shows the variation of flux density with the distance from the tangential beam port.

Table-3

Neutron flux distribution along the central line of the tangential beam port.

Neutron source	Foil mass (mgm)	Foil position (cm)	Activity at t=0, A ₀	Neutron flux, n/cm ² /sec
Reactor	60	0	1108.0	4.338×10^7
	62.9	50	651.4	2.435×10^7
	59.5	100	366.2	1.444×10^7
	58.9	140	272.2	1.085×10^7

Measurements were actually carried out at 400 Kwatts and then extrapolated to 3 MW_t these are shown in Fig. 5.



DISTANCE FROM THE TANGENTIAL BEAM PORT IN CM

FIG. 5

CHAPTER-3

RESULTS AND DISCUSSION

The neutron flux⁽⁸⁾ obtained at various distances in the central line of the tangential beam port from the biological shielding face of the research reactor is tabulated in Table-3. It is seen that as expected, neutron flux decreases as the distance from the biological shielding face of the reactor increases. Neutron flux was found to be maximum (4.338×10^7 n/cm²/sec) just at the surface of the biological shielding face of the reactor and minimum (1.085×10^7 n/cm²/sec) just before the beam catcher, which is placed at a distance of 140 cm. The photo peak efficiency of the high purity germanium detector measured for low intensity γ -ray of standard sources of known strength is given in Table-2. The efficiency as a function of energy is shown in fig.5. The resolution of the detector has been found to be 2.15 keV at 1332 keV gamma-ray from ⁶⁰Co source. It is seen from fig.5 that efficiency becomes maximum at energy 1.22 keV below which the efficiency decreases sharply. The efficiency, however, decreases more gradually above this value and becomes almost flat at higher energies.

In order to determine neutron flux from any source it is essential to measure very accurately the efficiency of the detector. Any uncertainty in the measurement of efficiency would introduce a large error in the determination of the neutron flux.

CHAPTER-4

STUDY OF NEUTRONS AND GAMMA-RAYS ATTENUATION PROPERTIES OF
MULTILAYER SHIELDS

4.1 INTRODUCTION

The primary purpose of shields is to protect personnel and equipment outside a reactor from the radiations that are produced inside. In addition, of course, other radioactive sources must be shielded as well. The shield which protects personnel is referred to as the biological shield^(35,36). Many layers of materials are usually placed between the reactive core itself and the outside of the shield, and all these attenuate the radiation and must be considered in a shield design. In principle, the radiations which might escape from a reactor include alpha and beta particles, gamma-rays, neutrons of various energies, fission fragments, and even protons resulting from (n,p) reactions. As far as shield design is concerned, however, only gamma-rays and neutrons need to be considered since these are by far the most penetrating. Any material which attenuates these radiations to a sufficient extent will automatically reduce all the others to negligible proportions. For the purpose of shield design, the neutrons and gamma-rays are considered from the standpoint of their place of origin: the primary radiations are defined as the radiation which originate within the reactor core due to nuclear fission, whereas the secondary radiations are produced outside the core as a result of the interaction of the primary radiations, chiefly the neutrons, with nuclei in the reflector, coolant, and shield materials. In this case, the radiation consists of a mixture of both gamma-rays and neutrons. As we have seen, elements of high atomic number are best for absorbing gamma-rays and elements of low atomic number are best for absorbing neutrons, so that there is no one element which is good

for both gamma-rays and neutrons. For this reason, the shield for a mixed radiation field must consist of a suitable mixture of heavy and light material/materials. In the present work a comparative study of the neutrons and gamma-rays using polyboron-heavy concrete, polyboron-ordinary concrete and polyboron-lead multilayered shielding arrangement have been studied.

4.2. REVIEW OF EARLIER WORKS

In a review article, Makarious et al ⁽⁹⁾ have studied of the penetration of primary gamma-rays, secondary gamma-rays and slow neutrons through an ilmenite-limonite (2.9 g/cm^3) shield and through both ordinary (2.3 g/cm^3) and ilmenite concrete (4.6 g/cm^3) shields. Source neutrons and gamma-rays were obtained from the ET-PR-1 reactor (2 MW). Experiments have shown that ilmenite concrete is better than both ordinary and ilmenite-limonite concrete for attenuation of gamma and slow neutrons.

Ueki and Namito ⁽¹⁰⁾ have determined an optimum arrangement for the neutron dose rate using iron-polyethylene slab shields by integral shielding experiments. They have observed the minimum dose point when the polyethylene slab was located near the detector with iron slab placed near the neutron source.

The attenuation and distribution of gamma-ray doses in a multilayered shield consisting of water, iron and ordinary concrete have been measured by Megahid et al ⁽¹¹⁾. The relaxation length of gamma-rays in ordinary concrete was evaluated. They have also measured the attenuation of reactor thermal neutrons in a bulk shield of ordinary concrete.

Maruyama et al⁽¹²⁾ have measured the broad beam attenuation coefficients of 4-32 MV X-rays in ordinary concrete, heavy concrete, lead and iron.

Bishop⁽¹³⁾ has measured flux density spectra and exposure build-up factor data for 6.2 MeV source photons penetrating two-layered shielding slabs composed of slabs of aluminium, steel and lead in six possible combinations. He found that shields with lead or steel as the outermost layer, the exposure build-up factor was lower than for lead only or steel only shields of the same mean free path (mfp) thickness. For shields with aluminium as the outer layer, the exposure build-up factor was higher than that predicted for aluminium only shields.

Yoshiaki et al⁽¹⁴⁾ has measured neutron and gamma-ray penetration in an iron shield at a 60 cm depth in a tightly coupled source shield configuration with the fast-neutrons from the reactor as a source. Rates of neutron reactions and gamma-ray dose rates in the iron shield were obtained using activation foils and thermoluminescent dosimeters. They calculated neutron and gamma-ray distribution, in the iron shield showing fairly good agreement with the experiments.

Gujrathi and D'auria⁽¹⁵⁾ have studied the attenuation of a fast (≈ 2.6 MeV) neutron beam by graphite, paraffin, polyethylene-boron, polyethylene-boron-lead, polyethylene-lithium and steel using an indirect method with a Ge(Li) gamma-ray spectrometer. In addition, the macroscopic removal cross-section for these materials were deduced. The effects of these materials on the thermal neutron flux were also observed.

Uwamino et al⁽¹⁶⁾ have measured the attenuation of neutrons and photons transmitted through ordinary concrete. Source neutrons and photons were obtained from Cf_{252} fission source. Relative shielding properties of amonia meta tungston for neutrons and gamma-rays from ^{252}Cf fission source have been studied by Senffle and Philbin⁽¹⁷⁾.

The attenuation of fast neutrons in ilmenite concretes has been studied by Adams and Lokan^(18,19). The densities of concretes studied varied from 2.4 to 3.8 g/cm³. No comparison has been made between ordinary concrete and ilmenite concrete.

Dubrovski et al⁽²⁰⁾ have studied the shielding properties of stone concretes by measuring the relaxation lengths, and they concluded that the stone concretes (density; 2.38 g/cm³) are more effective than the ordinary concretes (density: 2.2 g/cm³) from radiation shielding point of view.

F.U. Ahmed et al⁽²¹⁾ have studied the gamma-ray shielding properties of Ilmenite-Magnetite concrete and polyboron by measuring the instantaneous relaxation length and the spectral build-up factor using a Cf-252 source. Spectral build-up factor and instantaneous relaxation lengths have been fitted to the appropriate functions and the related co-efficients are also reported.

Bhuiyan et al⁽²²⁾ have studied the neutron transport and shielding properties of locally developed shielding material "POLYBORON". They measured the instantaneous relaxation length and effective removal cross-section as a function of penetration distance with and without cadmium sheet.

F.U. Ahmed et al⁽²³⁾ have measured the dose build-up factor (upto 20 mfp) for gamma-rays from a point isotropic ^{60}Co source penetrating multilayered concrete slabs using Cox's Bazar and Sylhet sands. They have also measured the instantaneous relaxation length for both types of concrete slabs. Results obtained show that the build-up factors for Sylhet sand slabs increase more rapidly than those of magnetic slabs.

Robsen and Kroon⁽²⁴⁾ have ~~studied~~ studied the attenuation of 14 MeV neutrons in concrete shields (density: 2.3 g/cm^3).

4.3 INTERACTION OF NEUTRONS WITH MATTER

There are two different modes by which neutrons may interact with matter. These are scattering and capture. When the neutrons are fast, there is a tendency for them to be slowed down by scattering processes. Scattering may be either elastic or inelastic and may be isotropic or non-isotropic. Elastic scattering, in which a neutron is deflected without loss of energy except for the kinetic energy which it imparts to the recoiling nucleus. Inelastic scattering, in which there is an interaction between the nucleus and the neutron resulting in the emission of a neutron with an energy different from that of the incident one. Capture, in which a neutron is absorbed into a nucleus which then undergoes some reaction (other than the remission of a neutron), usually the emission of a photon. A neutron can lose energy in a material as a result of elastic and inelastic scattering collisions with the nuclei of the material. If the neutron energy is less than the energy difference between the first excited

state and the ground state of the nucleus, then the neutron will lose energy by scattering collision. This is the principal mechanism for the slowing down of fission neutrons in materials. Elastic scattering is most important for light nuclei which can absorb a large fraction of the neutron's energy in recoil. Elastic scattering is possible for neutrons of all energies, but inelastic scattering can occur if the neutron energy is 10 MeV or higher so as to produce an excited state of the nucleus. This process always takes place through the formation of a compound nucleus. The importance of inelastic scattering is that the neutron energy is strongly degraded since it loses not only the energy equivalence of the recoil energy of the nucleus but also the energy equivalence of the inelastic scattering gammas. Inelastic scattering is more important for heavy nuclei because their allowable energy levels are more numerous.

Capture processes (n, γ) are very common and almost invariably occur more readily with slow neutron than with fast neutrons. In most materials, the capture reaction [or (n, γ) reaction] is the most probable, and plays an important part in the attenuation of neutron intensity and hence in the shielding of neutrons. The attenuation of neutrons may be summarised in the following manner:

At first, a high energy neutron passes through the absorber material and is slowed down by elastic or inelastic scattering. When the neutron has been slowed down to thermal energy, probability of capture reaction increases and the neutron will be completely absorbed with the emission of either a charged particle or a gamma-ray having an energy upto

several MeV. Since the neutron capture cross-sections for all materials is virtually zero at high energies, it is only when the neutron has reached sufficiently low energy that the capture of the neutron can take place. The probability of any one of these events occurring in a material is expressed quantitatively by their respective cross-section. The cross-section may be either large or small depending on the neutron energy. Inelastic scattering is an important mechanism in the degradation of the energy of fast neutrons. The cross-section for this process increases with the neutron energy and with the atomic number of the material in which the scattering occurs. This is an important characteristic in the shielding against fast neutrons.

Elements of low mass number is often used as the shield for slowing down neutrons of high energy, the cross-section for scattering is, however, small especially for elements of low mass number. It is then advantageous to utilize inelastic scattering by introducing an element (or elements) of moderate or high mass number. Hence, a combination of a moderately heavy or heavy element with hydrogen will effectively slow down even neutrons of very high energies. Although hydrogen alone (as water) could be used as a neutron shield, a shield consisting entirely of hydrogen in the form of heavy water would be unsatisfactory. A single inelastic scattering collision would decrease the neutron energy to about 1 MeV or less, but subsequent collisions would be elastic in nature. Many such collisions would then be necessary to reduce the neutron energy to a value at which the capture cross-section is significant. In the mean

time, the neutron would have penetrated a considerable distance into the shield. The next aspect of reactor shielding to consider is the capture of neutrons after they have been slowed down. Actually this is a relatively simple matter, even though the shield does not contain an element with large or fairly large cross-section for the capture of slow neutrons. In fact, it is generally accepted that in a shield containing sufficient hydrogen, almost every neutron which has suffered inelastic scattering may be regarded as removed, since the probability of further slowing down and subsequent capture is large.

4.4 INTERACTION OF GAMMA-RAYS WITH MATTER

There are three ways in which gamma-rays interact with matter; the photoelectric effect, the Compton effect, and pair production. These interactions have already been discussed in section (1,2,6).

4.5 DEFINITION OF SOME NUCLEAR PARAMETERS

To evaluate the effectiveness of any new shielding material, the following nuclear parameters should be measured:

- i) Attenuation coefficient (μ)
- ii) Removal cross-section (Σ_R)
- iii) Half value thickness (HVT)
- iv) Relaxation length (λ) and
- v) Build-up factors (B).

Each of the term mentioned above is briefly described below:

ATTENUATION COEFFICIENT (μ)

The most important quantity characterizing the penetration and diffusion of gamma radiation in extended media is the attenuation coefficient, μ . This quantity depends on the photon energy E and on the atomic number Z of the medium, and may be defined as the probability per unit path length that a photon will interact with the medium. The rate at which gamma-rays are attenuated is determined primarily by the atomic number and density of the shielding material, and to a lesser extent by its geometrical configuration. Let us consider a slab of material of thickness t located between a narrowly collimated beam of monoenergetic gamma-ray photons and a narrowly collimated detector, as shown in fig. 6. The distinctive feature of a narrow beam experiment (i.e., one having 'good geometry') is that only the photons which traverse the specimen absorber without experiencing an interaction of any kind, reaches the detector; all other photons are prevented from reaching the detector. When monoenergetic gamma-ray photons traverse a small thickness of slab at any point in a medium, the extent of interaction of the photons is proportional to the radiation intensity at that point and to the thickness traversed. Consequently, in traversing the distance dt , the intensity of the gamma-ray photons which have not undergone interaction will be decreased by

$$\frac{dI}{I} = - \mu dt \quad \dots \quad (4a)$$

where μ is called the attenuation coefficient of the absorber for the given radiation. Integrating eqn (4a) and assuming that the beam intensity incident on the slab has the value $I(0)$, the intensity transmitted $I(t)$ through the slab of a homogeneous medium is given by

$$I(t) = I(0)e^{-\mu t} \quad \dots \quad (4b)$$

Eqn. (4b) represents the attenuation of gamma-rays in a material medium and is exponential in nature.

REMOVAL CROSS-SECTION (Σ_R)

The removal cross-section of a material, as used in the shielding calculations, is the cross-section which describes the probability that a fast neutron will reach a given detection point in a material without being absorbed or scattered out of the direct path. If t is the thickness of the material through which fast neutrons are passing, then (neglecting geometry effects) the ratio of the emergent (transmitted intensity), $I(t)$ to the incident intensity, $I(0)$ is given by

$$I(t) = I(0)e^{-\Sigma_R t} \quad \dots \quad (4c)$$

where Σ_R is the macroscopic removal cross-section for neutrons in the material, but it is not a cross-section in the sense of representing the probability of a particular neutron-nucleus interaction. The observed value of the removal cross-section is, in fact, roughly equal to two-thirds of the total (scattering and capture) cross-section in the given material for neutrons having energies in the range of 6 to 8 MeV.

HALF-VALUE THICKNESS (HVT)

The absorption effect of radiation by shielding materials may be characterized, by their half-value thickness (HVT), which is the thickness required to reduce the intensity (or initial number of counts) to one-half. Similarly, the tenth-value thickness (TVT) is the thickness required to reduce the intensity to one-tenth. These quantities can be evaluated graphically from the experimental beam attenuation curves, by plotting the transmitted intensity against the corresponding thickness of the absorbing materials.

RELAXATION LENGTHS (λ)

The relaxation length of any material is that thickness of material in which the incident radiation diminishes to a factor of $\frac{1}{e}$ (i.e., $\frac{I(t)}{I(0)} = \frac{1}{e} = 0.368$) or to 37% of its incident intensity, where e is the base of natural logarithms. This factor is also called the mean free path (mfp), which represents the average distance traveled by a photon between successive interactions. If $I(t)$ is the radiation (neutron or gamma-ray) flux or related quantity at a point t within a shield, then the relaxation length λ , for the given radiation and medium, is given by

$$\frac{1}{\lambda} = - \frac{1}{I(t)} \frac{dI(t)}{dt} \quad \dots \quad (4d)$$

at the point t . As defined in this manner, the relaxation length may vary with the distance t within the shield. However, it is often found

that, owing to a combination of circumstances, the radiation flux decreases in an approximately exponential manner over a range of distances in the shield; over this range λ remains constant and the flux at t can be represented by

$$I(t) = I(0)e^{-t/\lambda} \quad \dots \quad (4e)$$

where $I(0)$ is the flux at the origin of the t co-ordinate. Comparison with the attenuation equation for gamma-rays (4b) and equation for neutrons (4c) shows that λ is formally equivalent to $\frac{1}{\mu}$ or $\frac{1}{\Sigma_R}$, respectively. Since the relaxation length of a particular radiation in a given material is equivalent to the reciprocal of an attenuation coefficient (for gamma-rays) or a removal cross-section (for neutrons), it is dependent on the energy of the radiation. For a specified radiation of a given energy, the relaxation lengths (or their reciprocals) provide a rough means for comparing the shielding effectiveness of different materials. Relaxation lengths may also occasionally be used in very preliminary shielding calculations, but this procedure is not recommended unless there is a clear understanding that the results are highly approximate.

BUILD-UP FACTOR (B)

In the exponential law (eqn.4b) for the attenuation of gamma-radiations in a material, it is assumed that the particular photon involved in a reaction such as photoelectric effect, Compton scattering and pair production in the material is completely eliminated and is not seen by a

detector put across the shielding material. It is however, true only in the case of narrow beam geometry (Fig.6a). In the case of broad beams of radiation (Fig.6b), the secondary radiations resulting from the interaction of primary photons in the material have every possibility to pass through the shield and thus the photon flux across the shield will be greater than that calculated from eqn.(4b). In the case of broad beams the eqn.(4b) will be modified to

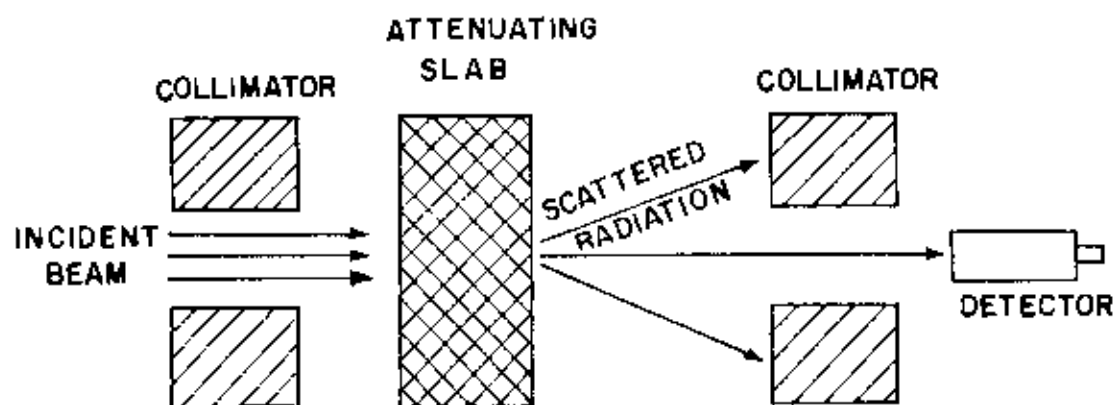
$$I(t) = BI(0)e^{-\mu t} \quad \dots \quad (4f)$$

where B is the build-up factor and is defined as follows⁽⁴⁴⁾.

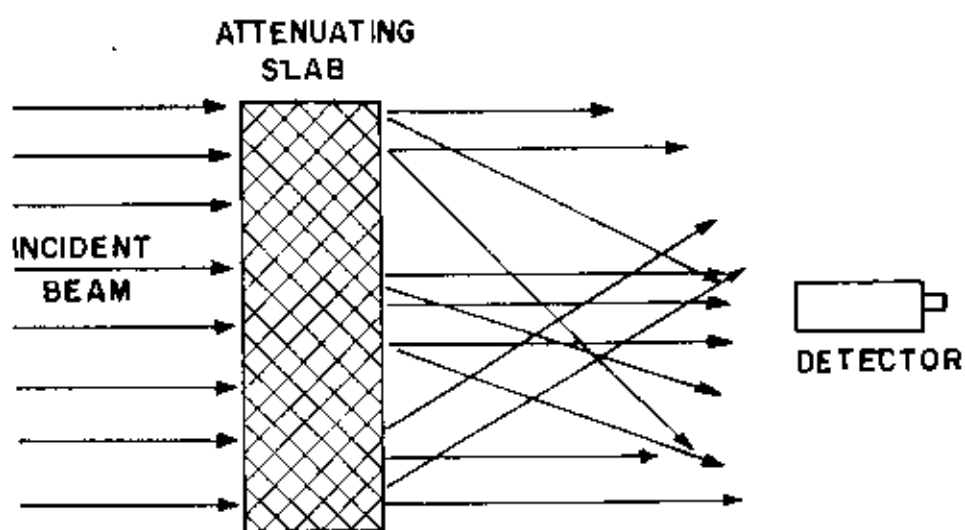
$$B = \frac{\text{Quantity of interest at a point due to the total number of particles}}{\text{Quantity of interest at a point due only to non-interacted particles}}$$

The "quantity of interest" might be the number of particles, their energy, or the dose imparted by them; thereby giving rise the number, energy, and dose build-up factors, respectively. The build-up factor, B, takes into account the increase in the radiation intensity due to scattering within the absorber. Let $I(0)$ is the initial intensity of the radiation source, $I(t)$ is the attenuated intensity after passing through the shielding materials of thickness $t(\text{cm})$ and μ is the attenuation coefficient (cm^{-1}). If all three types of interaction of gamma-ray photons with the matter are included, then

$$\mu = \mu_{pe} + \mu_c + \mu_{pp} \quad \dots \quad (4g)$$



(a)



(b)

FIG. 6. EXPERIMENTAL ARRANGEMENTS FOR MEASUREMENTS OF ATTENUATION COEFFICIENT

(a) NARROW BEAM OR GOOD GEOMETRY AND

(b) BROAD BEAM OR POOR GEOMETRY.

where μ_{pe} , μ_c and μ_{pp} represent the attenuation coefficients due to photoelectric, the Compton effect, and pair production, respectively. Usually, build-up factors are given at different relaxation lengths or attenuation units, μt . Like the attenuation coefficient, the value of the B varies with absorber material and radiation energy. It also varies with geometry of the source and depth of penetration in the absorbing material. The total attenuation coefficient is calculated for a given energy by

$$\mu = \frac{0.693}{HVT} \dots \quad (4h)$$

where HVT is the half value thickness. In ~~practical gamma-ray shielding~~ calculation, the build-up factor is being widely used to determine the total effect of the radiation at the point of interest. In principle the build-up factor concept is also applicable to neutron attenuation, but in practice it is found to be much less successful when applied to neutrons, and consequently it is much less important a concept in the context of neutron shielding calculation.

CHAPTER - 5

EXPERIMENTAL METHOD

5.1 EXPERIMENTAL SETUP.

The measurement of attenuation properties of neutrons and gamma-rays through different types of arrangements of multilayer shields were carried out at the laboratory of the Institute of Nuclear Science and Technology (INST) of the Atomic Energy Research Establishment (AERE), Savar. In this experiment, radiation transmission measurements were made for 'broad beam' geometry conditions, i.e., the shielding material being studied was placed directly adjacent to the detector. This type of geometry allows the detection of the increased radiation due to Compton scattered photons from the attenuating material. A block diagram of the experimental setup, for the measurement of attenuation properties (both neutrons and gamma-rays) along with the schematic diagram is shown in Fig.7.. The experimental set up consists of a radiation source, a detection system and multilayer shielding materials. The distance between the source and the detector was 118 cm. Since the materials are meant to be used as a shield for a reactor, the radiation chosen was ^{252}Cf which emits fission neutrons with an average energy 2.3 MeV⁽²⁵⁾, and numerous gamma-rays from fission products (<3 MeV). This is almost identical to those of uranium-235 fission. The detection system consists of two parts: a detector and a recording system. The incoming radiation interacts with the detector and gives rise to an output pulse. The recording system receives this output pulse and after proper amplification and subsequent discrimination, records the number of events. The method used for the detection of neutron and gamma radiation depends on the ionization produced in the detector in course of their

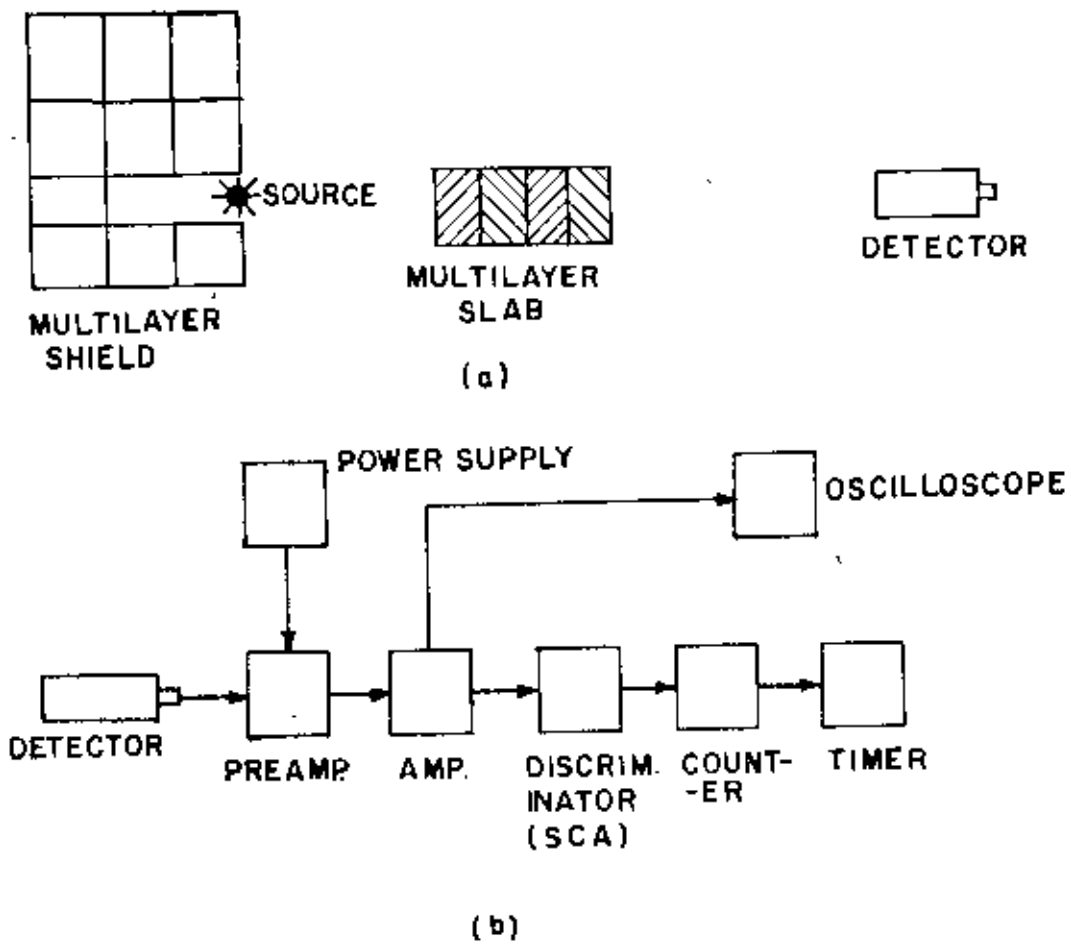


FIG. 7. (a) A BLOCK DIAGRAM OF EXPERIMENTAL SET UP. AND
 (b) ELEMENTS OF A TYPICAL SIGNAL CHAIN FOR
 PULSE COUNTING.

passage through the gas and matter, respectively. In the interaction of gamma radiation with matter, ion-pairs are produced. Similarly, neutrons are detected through nuclear reaction which results in energetic charged particles (such as protons, alphas and so forth) that reveal their presence by ionization they produce. The gamma-ray intensity was measured with a portable NaI (Tl) scintillation detector. Measurements of neutron intensity were carried out using a long counter, which was constructed following the design of Hanson-McKibben⁽²⁶⁾, incorporating the modification of thickness of the paraffin moderator as suggested by other workers⁽²⁷⁾. The long counter used in this study was a BF_3 gas proportional detector surrounded by cylindrical paraffin moderator to monitor neutron flux. Its sensitivity is reasonably uniform for neutron energies ranging from thermal to 10 MeV. This device has proved to be highly successful as a neutron monitor in experiments using fast neutrons.⁽²⁸⁾ The operating voltage of the BF_3 gas proportional detector was 1850 volts (Fig.8). In these measurements polyboron, heavy concrete, ordinary concrete and lead slabs were used as shielding materials. The dimensions of the slabs are shown in Table-4. Out of these four materials, three types of multilayer shielding arrangements were used. These are polyboron-heavy concrete, polyboron-ordinary concrete and polyboron-lead shields.

Table-4
Dimension of the single layer slabs

Material	Thickness (cm)	Width (cm)	Height (cm)
Heavy Concrete	5	25.5	12.5
Ordinary Concrete	5	25.5	12.5
Polyboron	4.1	20	10
Lead	5.2	20	10

The intensity of incident neutrons and gamma-rays was first measured without placing any shielding material between the source and the detector. Then the first shielding arrangement of polyboron backed by heavy concrete slabs was placed nearest to the source and the intensity of the transmitted neutrons or gamma-rays was measured. Next more slabs of polyboron backed by heavy concrete were successively introduced behind the already existing slabs and the corresponding intensities of transmitted neutrons or gamma-rays were measured. In this manner, the multilayer shielding thickness was successively increased while the rest of geometry remained unchanged. The measurements were repeated till the total thickness of polyboron backed by heavy concrete increased up to a maximum of 91 cm, the total thickness of polyboron being 41 cm and that of heavy concrete being 50 cm. This enables one to study the deep penetration behavior of neutrons and gamma-rays for the multilayer shielding materials.

The experiment was repeated for the other two shielding arrangements. In the arrangement of polyboron backed by ordinary concrete slabs, the total thickness used was 91 cm (polyboron-41 cm and ordinary concrete-50 cm.), while in the arrangement of polyboron backed by lead slabs, the total thickness used was 92 cms (polyboron-41 cm lead-52 cm). The detailed description of the detectors, the radiation source and the slab materials used in these experiments are furnished in the sections(5.2, 5.3, 5.4, 5.5). Brief descriptions of some of the different components of the electronics circuitry have already been given in sections(1.2.2, 1.2.3). The rest are described briefly below,

LINEAR AMPLIFIER

Two primary functions are conveniently provided by the linear amplifier element in the pulse processing chain: pulse shaping and amplitude gain. The unit accepts tail pulses as an input, often of either polarity, and produces a shaped linear pulse with standard polarity and span-width. The amplification factor or gain depends on the particular application, but generally lies between a factor of 100 to 5000. The gain is normally adjustable over a wide range through a combination of coarse and fine controls. A good amplifier should have low noise input and be capable of amplifying pulses with rise time of the order of 10^{-8} second. In this present study Canberra Model 2012 amplifier was used. Its salient features are as follows:

- O Gain : 1280
- O Designed for sodium iodide scintillator, gas proportional,

and silicon surface barrier detectors

- O High performance spectroscopy amplifier
- O Low noise
- O Selectable time constants
- O Count rate optimization, etc.

DIFFERENTIAL DISCRIMINATOR (SINGLE CHANNEL ANALYZER)

In order to count the pulse properly, the shaped linear pulses must be converted into logic pulses. One of this is a differential discriminator or single channel analyzer (SCA) which produces a logic output pulse only if the input linear pulse amplitude lies between two levels. The action of the unit is therefore to select a band of amplitudes or 'window' in which the input amplitude must fall in order to produce a recordable event. The discrimination level is normally adjustable by a front-panel control. In some units, the lower level discriminator (LLD) and upper level discriminator (ULD) are independently adjustable from front-panel controls. In counting systems, the SCA can serve to select only a limited range of amplitudes from all of those generated by the detector. In many counting situations, the level is set just above the system noise so that the maximum sensitivity for counting detector pulses of all sizes is realized. In this experiment Canberra Model 2030 SCA was used.

TIMERS AND COUNTERS

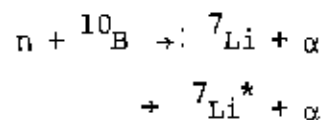
The function of a timer is simply to start the counting and select the accumulation period for an electronic counter or other recording system after which the counting automatically stops. Obviously its most important property is the precision to which the time interval is controlled. The precision of the timing is determined solely by the accuracy and stability of the power line frequency. Timers, can be either blind or have display units. It may be convenient to have the accumulated timing period displayed during the course of the measurement, although the feature adds to the cost of the timer.

As the final step in a counting system, the logic pulses must be accumulated and their number recorded over a fixed period of time, set by the timer. The device used for this purpose may be a simple digital register which is incremented by one count each time a logic pulse is presented to its input. In nuclear pulse counting applications, such devices are often called scalars. Counters are commonly operated in one of two modes: preset time and preset count. It can also be of the 'blind' or 'display' type.

In the present work Canberra Model 2071A Dual timer/counter was used. It provides two eight decade counter, a crystal time base, and presetting logic. The Model 2071A accommodates input counting rates of 100 million counts per second (100 MHz) for negative inputs and 25 million counts per second (25 MHz) for positive inputs.

5.2 NEUTRON DETECTOR

Neutron cannot be detected directly since they have no charge to produce ionization, it can only be detected by means of secondary charged particles such as protons, alphas, and so forth which may be released during its passage through matter, or by other secondary processes which produce ionizing radiation. Different types of detectors are available for measuring fast neutrons⁽²⁹⁾. The commonly used are liquid scintillation detectors, nuclear emulsion, threshold detectors, ^3He or ^6Li sandwich detectors, and proton-recoil detectors. In addition, there exist several fast neutron detectors based upon the slowing down of fast neutrons and then measuring these slow neutrons. A widely used detector for slow neutrons is the BF_3 detector. Boron trifluoride gas serves both as the target material and the counting gas. A BF_3 detector usually consists of a cylindrical outer tube of stainless steel, aluminium or copper and a central anode wire of nickel or tungsten. The usual operating voltage of the detector is in the range of 2000 to 3000 volts with the anode wire diameter of about 0.05 mm. Figure 8 shows count rate versus anode voltage curve for a typical case. The most common reaction for the conversion of slow neutrons into directly detectable particles is the $^{10}\text{B}(n, \alpha)$ reaction. The reaction may be written as



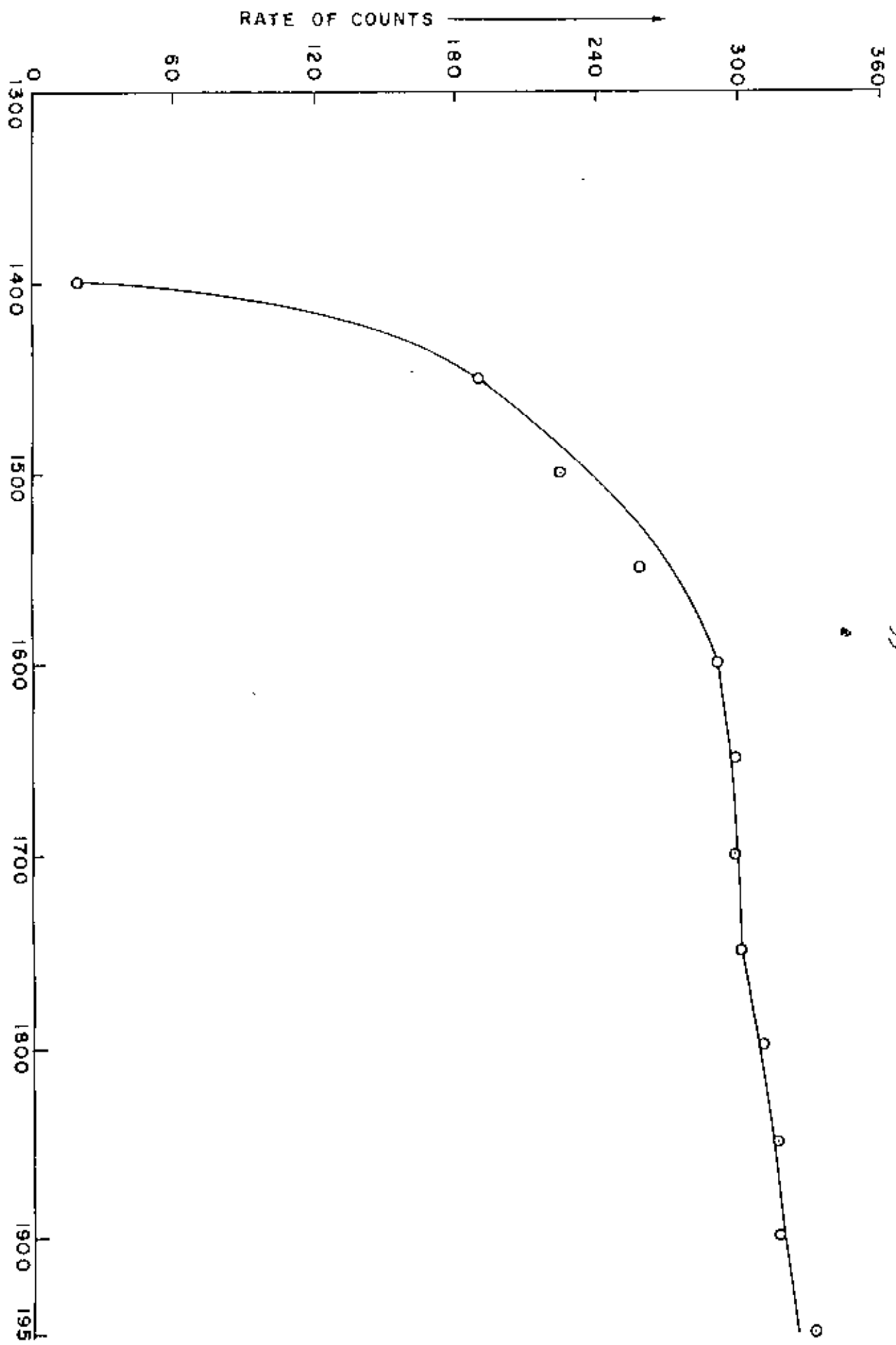


FIG. 8

which has a thermal cross-section of 4000 barns for ^{10}B isotope reaction. When thermal neutrons (0.025 eV) are used to induce reaction, about 94 percent of all reactions lead to the excited state and only 6 percent directly to the ground state. In the $^{10}\text{B}(n,\alpha)$ reaction, the energy of 2.31 MeV is shared by the alpha particles and the recoiling ^7Li nucleus of which alpha particle carries away 1.47 MeV and the ^7Li nucleus retains 0.84 MeV as the kinetic energy and the rest if any, as excitation energy. The thermal neutron cross-section for the $^{10}\text{B}(n,\alpha)$ reaction is 3840 barns. The slow neutron measurements were made with a BF_3 detector which feeds into a standard amplifier and scaling circuit. Since BF_3 detectors are mostly used only for counting the number of slow neutrons (0.5 MeV) which are detected, the distribution of the pulse heights of the detector is of little interest except that one has to ensure that all the resulting pulses from the detection of neutrons lie much above the electronic noise and the small background pulses resulting from the gamma-rays. It is to be noted, however, that the pulse height spectrum has significant number of counts at pulse heights which are much lower than that corresponding to the full energy peak. These lower amplitude pulses arise due to nuclear reactions taking place near the wall of the chamber in which one of the charged particles deposits only part of its energy in the gas and the rest being deposited in the counter wall. The particle which loses energy in the counter wall can be either the alpha particle or the lithium ion and the corresponding spectrum is of the type as shown in figure 9. The wall effect continuum extends from E_{Li} (0.84 MeV) up to full-energy peak at $(E_{\text{Li}} + E_{\alpha})$ (2.31 MeV). We

have considered only those reactions leading to the ${}^7\text{Li}$ excited state because the wall effect continuum associated with the much less probable ground state is normally so small as to be submerged by the remainder of the spectrum. The BF_3 tube of a detector from which the differential pulse height spectrum tells us nothing about the energy spectrum of the incident radiation, but is a function of only the size and geometry of the detector itself. Instead, we are likely to seek a stable operating point of a counting plateau for which small drifts in operating parameters do not significantly affect the neutron sensitivity of the counter. That objective would be met by setting a fixed discriminator level at the point labeled A in figure 9. The flattest portion of that plateau should occur when the effective discrimination point is at the minimum in the differential pulse height spectrum or point A. Under these conditions, all the neutrons will be counted, whereas low-amplitude events will be rejected. A very important consideration in many applications of BF_3 tubes is their ability to discriminate against gamma-rays which often are found together with the neutron flux to be measured. Gamma-ray interact primarily in the wall of the counter and create secondary electrons which may produce ionization in the gas. Because the stopping power for electrons in gases is quite low, a typical electron will deposit only a small fraction of its initial energy within the gas before reaching the opposite wall of the counter. Thus we should expect that most gamma-ray interactions will result in low-amplitude pulses which will lie in the tail to the left of point A in figure 9. Simple amplitude discrimination can then easily eliminate

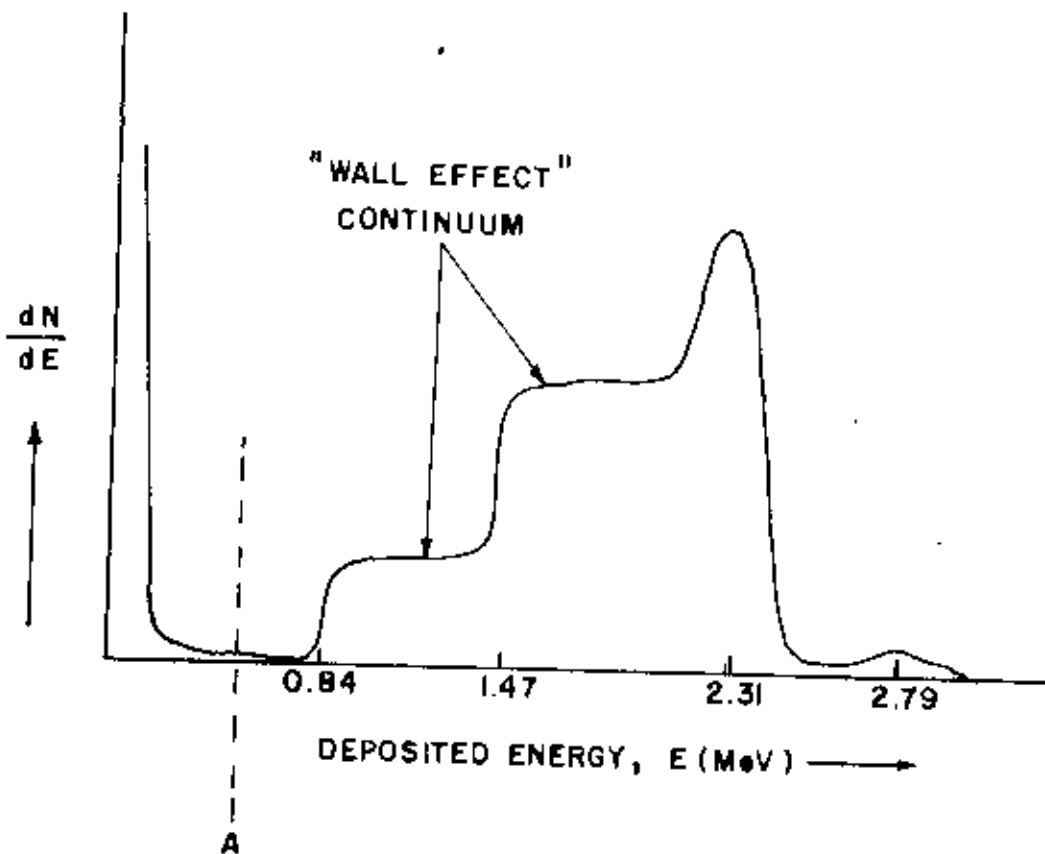


FIG. 9. EXPECTED PULSE HEIGHT SPECTRA FROM BF_3 TUBES ILLUSTRATES THE ADDITIONAL CONTINUUM DUE TO THE WALL EFFECT.

this gamma-rays without sacrificing neutron detection efficiency. The detection efficiency for neutrons incident along the axis of a BF_3 tube is given approximately by ⁽²⁹⁾;

$$\epsilon(E) = 1 - \exp \left[- \Sigma_a(E)L \right] \quad \dots \quad (1)$$

where $\Sigma_a(E)$ is the macroscopic absorption cross-section of ^{10}B at energy E and L is the active length of the tube. Using equation (1), the calculated efficiency for a 30 cm long BF_3 tube (96 percent enriched in ^{10}B) is 91.5% at thermal neutron energies (0.025 eV) but drops to 3.8% at 100 eV. Thus, a BF_3 tube exposed to neutrons with mixed energies will respond principally to the thermal neutron components and will have extremely low detection efficiency for fast neutrons. The specifications of this detector are shown in Table-5.

Table-5


 BF_3 detector specifications

Manufacturer	:	Canberra Inc.
Model	:	4528
Diameter	:	2.54 cm
Anode	:	0.005 cm diameter tungsten
End window	:	0.203 cm thick alumina (Al_2O_3)
Fil gas	:	BF_3 (90% ^{10}B) at 120 cm Hg.
Active length	:	30 cm
Outer sheel	:	0.089 cm thick

As a rule, however, fast neutron devices must employ a modified or completely different detection scheme to yield an instrument with acceptable detection efficiency. Conventional BF_3 tubes have an extremely low detection efficiency for fast neutrons, and consequently are almost never used for this purpose. The inherently low detection efficiency for fast neutrons of any slow neutron detector can be somewhat improved by surrounding the detector with a few centimeters of hydrogen-containing moderating materials. The incident fast neutron can then lose a fraction of its initial kinetic energy in the moderator before reaching the detector as a lower energy neutron, for which the detector efficiency is generally higher. By making the moderator thickness greater, the number of collisions in the moderator will tend to increase, leading to a lower value of energy when the neutron reaches the detector. One would therefore expect the detection efficiency to increase with moderator thickness if that were the only factor under consideration. A second factor, however, tends to decrease the efficiency with increasing moderator thickness. The probability that an incident fast neutron ever reaches the detector will inevitably decrease as the moderator is made thicker. A neutron may be absorbed within the moderator before it has a chance of reaching the detector. The absorption probability will increase rapidly with increasing moderator thickness because absorption cross-sections generally are larger at lower neutron energies. The efficiency of a moderated slow neutron detector when used with a monoenergetic fast neutron source will thus show a maximum at a specific moderator thickness. A detector whose counting

efficiency does not depend on the neutron energy can be very useful device in many areas of neutron physics. For an ideal detector of this type, a graph of the detection efficiency versus neutron energy is a horizontal line, which has led to the name flat response detectors. The most popular flat response neutron detector has been the so-called "Long Counter". Like the spherical neutron dosimeter⁽³⁰⁾, it is based on the principle of placing a slow neutron detector at the center of a moderating medium.

The combination of a BF_3 tube and cylindrical moderator was first suggested as a flat response neutron detector by Hanson and McKibben⁽²⁶⁾. Thies and Botcher⁽³¹⁾ demonstrated how one can construct a flat response fast neutron detection system using a larger moderator with a BF_3 detector embedded in it in a suitable geometry. A latter design by McTaggart⁽²⁷⁾ is shown in figure 10a and has achieved fairly widespread acceptance as the standard long counter. The counter is designed to be sensitive only to neutrons incident on the right-hand face of the counter within the boron oxide shell. Those incident from other directions tend to be moderated by the outer annulus of paraffin, and are subsequently captured in the boron layer without giving rise to a count. Neutrons which are incident on the front face parallel to the cylindrical axis will penetrate some distance before undergoing moderation. The average distance of penetration will increase as the neutron energy increases. If the BF_3 tube and cylindrical moderator are sufficiently long, then the typical cross-section through the cylinder at the point of moderation will not be

different for various energy neutrons. Therefore, the probability that the moderated neutron will find its way to the BF_3 tube and produce a count which is independent of neutron energy. It is this property that leads to the flat energy response of the detector. Figure 10a shows the long counter which was constructed following the design of Hason and McKibben⁽²⁶⁾ incorporating the modifications suggested by other workers⁽³¹⁻³³⁾. A typical efficiency curve versus neutron energy of a modified long counter⁽¹⁾ as shown in fig.10b. In the diagram of the long counter shown in figure 10a. The conventional BF_3 proportional counter tube was embeded in a large cylindrical  paraffin moderator 50.8 cm(20") in length and 38.1 cm (15") in diameter. The moderator had eight 2.54 cm (1") diameter holes, 8.89 cm (3.5") deep, in its front face, on a circumference 22.86 cm (9") in diameter. The holes provided in the front surface prevent a fall off in the efficiency at neutron energies below 1 MeV by allowing the lower energy neutrons to penetrate further into the moderator. The inner paraffin cylinder is 20.32 cm(8") in diameter and the density of the paraffin wax is 0.84 g/cm^3 . The BF_3 detector used in this study was Canberra Model 4528 (Table-5), which had an active length as that of the paraffin cylinder, and was filled at 120 cm Hg. pressure with enriched BF_3 . A cadmium cap covered the front end of the BF_3 detector. The outside of the paraffin may be covered with a thin sheet of cadmium to absorb thermal neutrons while allowing fast neutrons to pass through in to the paraffin.

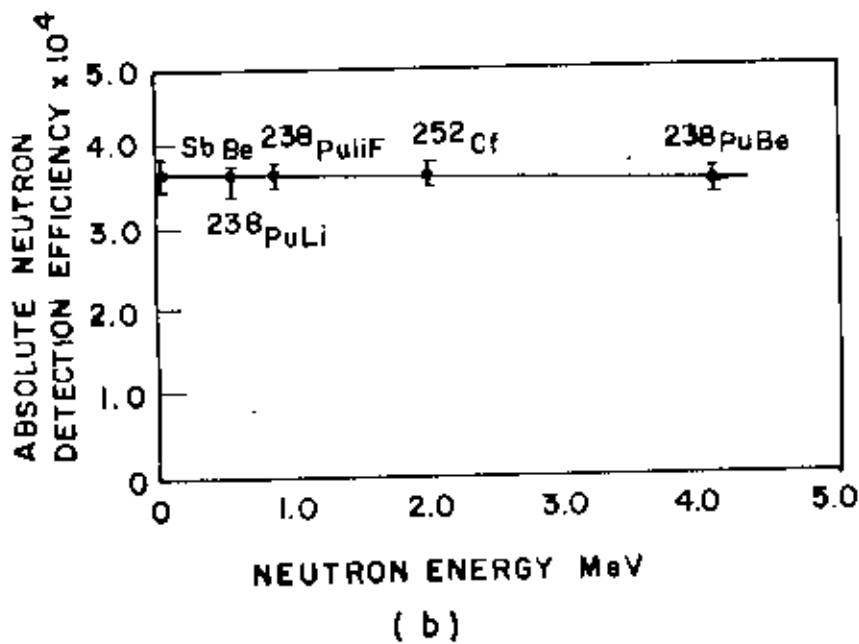
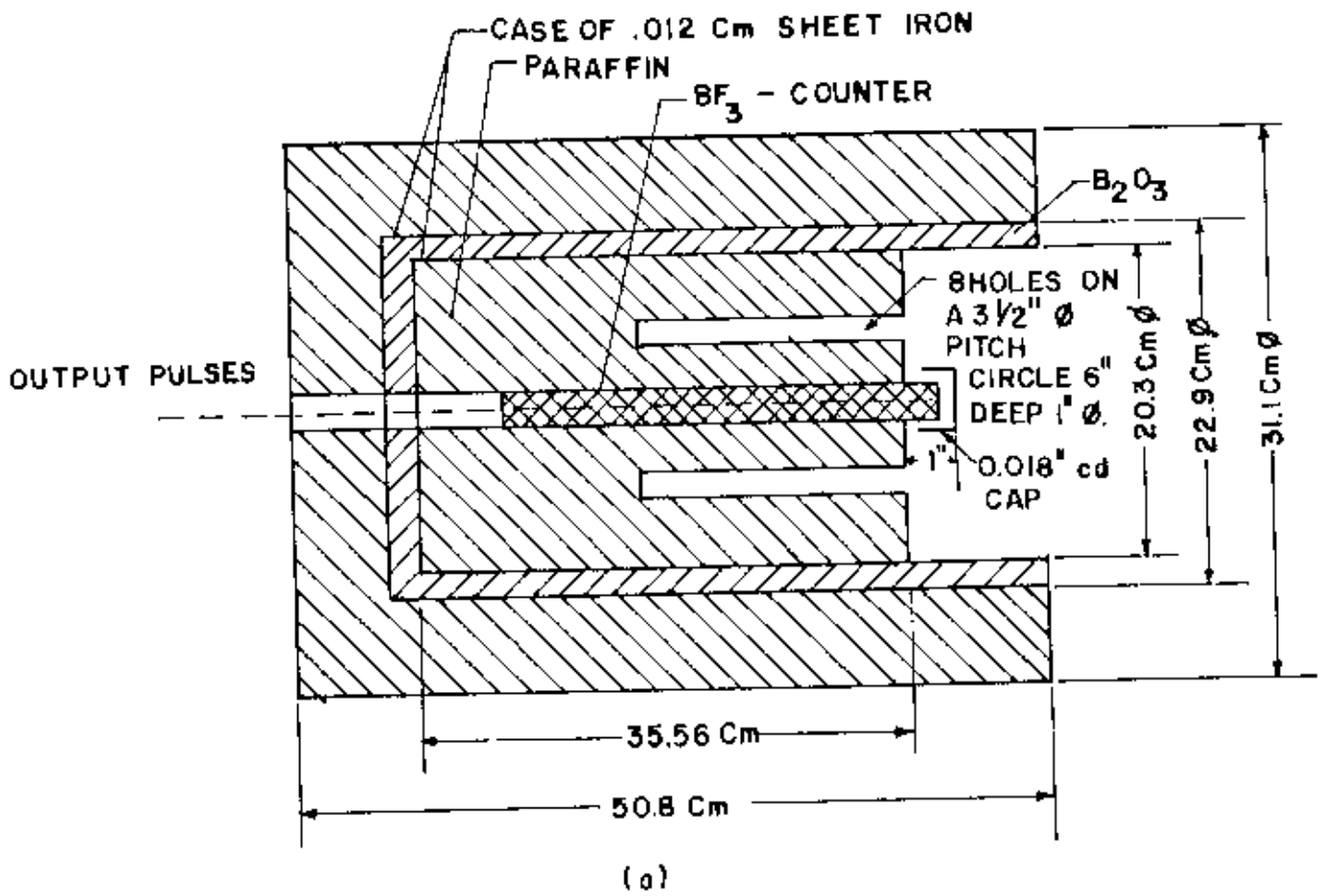


FIG. 10 (a) CROSS SECTION OF THE LONG COUNTER AND
 (b) A TYPICAL EFFICIENCY CURVE OF THE LONG COUNTER.

5.3 GAMMA-RAY DETECTOR

A gamma-ray photon is uncharged and creates no direct ionization or excitation of the material through which it passes. The detection of gamma-rays is therefore, critically dependent on causing the gamma-ray photon to undergo an interaction that transfers all or part of the photon energy to an electron in the absorbing material. There are three principal methods in which the gamma-ray photons interact with matter. These are photoelectric effect, Compton scattering, and pair production. These processes already discussed in section 1.2.6 are strongly dependent upon the energy of the gamma-ray photon and the atomic number of the material. In summary, all three processes produce moving electrons (or positrons) in matter, which can be detected directly or can initiate other electron processes to obtain an electric charge pulse. At low energy, up to about 100 keV, the photoelectric effect is dominant. Compton scattering varies from minor effect at 10 keV to being more important near 100 keV. Up to 1 MeV the photoelectric effect is declining in probability and multiple Compton scattering effects become important. Above 1.02 MeV pair production increases in probability. Since the primary gamma-ray photons are "invisible" to the detector, it is only the fast electrons created in gamma-ray interactions that provide the only clue to the nature of the incident gamma-rays. These electrons have a maximum energy equal to the energy of the incident gamma-ray photon, and will slow down and lose their energy in the absorption processes. Energy loss is, therefore, through ionization and excitation of atoms within the absorbing material. For a detector to serve as a gamma-ray spectrometer, it must carry out two distinct functions. First,

it must act as a conversion medium in which incident gamma-rays have a reasonable probability of interacting to yield one or more fast electrons, and second, it must function as a conventional detector for these secondary electrons. A wide variety of detectors⁽³⁴⁻³⁷⁾ are in use today. The most widely used detectors include the inorganic alkali halide crystals, of which sodium iodide is the favorite, and organic-based liquids and gases which emit lights from their atoms or molecules (or scintillates) when excited by the passage of radiation through them. Hence, these detectors are commonly referred to as scintillators. This process of absorption of energy by a substance and its re-emission as visible or near-visible radiation are known as luminescence^{which is of two kinds-phosphorescence and fluores-}cence. The process where the light emission occurs during the excitation or within 10^{-8} sec or less the radiation is called fluorescence. When the excited state is metastable, the light emission is delayed (of the order microseconds to hours) and the luminescence is known as the phosphorescence. Only those scintillators in which light emission occurs within the shorter duration (10^{-12} sec) are useful for the detection of nuclear radiation. The desirable properties for a good scintillators may be summarized as follows:

- density should be high to make it a suitable material for efficient absorption of electro-magnetic radiation
- should be highly fluorescent with very little or no phosphorescence
- the emission spectrum should be suitable for good matching to all types of commercial photomultipliers available

0 should fluorescence which means inherently good resolution

The inorganic scintillators are crystals of inorganic salts, primarily the alkali halides, containing small amount of impurities as activators for the luminescence process. The scintillation mechanism in inorganic materials depend on the energy states determined by the crystal lattice of the material. When the gamma-ray passes through a scintillator, a part or all of its energy is absorbed in the scintillator. In inorganic scintillator, this absorbed energy can raise molecule from their electronic ground states to their electronic excited states. A molecule in the electronic excited state may lose its energy to lattice vibrations or may return to its electronic ground state with the emission of visible light. The luminescence of an organic scintillator is an electronic process which may be represented in the band theory by the lower band, called the valence band, which represents those electrons that are essentially bound at lattice sites, whereas the conduction band represents those electrons that have sufficient energy to be free to migrate through out the scintillator. There exists an intermediate band of energies, called the forbidden band, in which electrons can never be found in the pure scintillator. Absorption of energy can result in the elevation of an electron from its normal position in the valence band across the gap into the conduction band, leaving a hole in the normally filled valence band. In the pure crystal, the return of the electron to the valence band with the emission of photon is an inefficient process.

In order to enhance the probability of visible photon emission during the de-excitation process, small amount of an impurity are commonly added to inorganic scintillators. These impurities, called "activators" create special sites within the pure crystal. As a result there will be energy states created within the forbidden gap through which the electron can de-excite back to the valence band. Because the energy is less than that of the full forbidden gap, this transition can now give rise to a visible photon and therefore serve as the basis of the scintillation process. Energy band structure of an activated crystalline scintillator is illustrated in figure 11.

A number of inorganic scintillators (or phosphors) namely NaI(Tl), CsI(Tl), Li(Eu) etc. are in widespread use as scintillator detectors. The mechanical and physical properties of the scintillator, prepared in appropriate sizes and shapes, play an important part in their choice for specific measurements. The NaI(Tl) detectors have become standard scintillation detectors for gamma-ray spectroscopy since its introduction by Hofstadter⁽³⁸⁾ and Hilne⁽³⁹⁾. Sodium iodide is a transparent, hygroscopic crystal having the general properties at room temperature (300K). The thallium activator which is present as an impurity in the NaI crystal structure to the extent of about 0.2% enhances the conversion of energy absorbed in the crystal to light. Its high density (3.67 g/cm³) together with its high effective atomic number (Z = 53) makes it a suitable material for the efficient absorption of electromagnetic radiation. The presence of iodine gives high cross-section for photoelectric and pair production interactions. The emission

spectrum with a maximum of 4100 \AA is suitable for good matching to many types of commercial photomultiplier (PM). The speed of response makes it suitable for most applications, its decay time is of the order of 0.23 microsecond. Transparency to its own fluorescence provides NaI(Tl) with an inherently high energy resolution which can be achieved with a scintillator detector. Figure 12 shows a typical curve which explains the interaction processes of gamma-rays with NaI(Tl) crystal. The primary ionizing particles resulting from the gamma-ray interactions namely the photoelectrons, Compton electrons, and electron-positron pairs, dissipate their kinetic energy by exciting and ionizing the atoms in the crystal. The excited atoms return to the ground state by the emission of light quanta. The intensity of the light flash produced in the scintillator is proportional to the amount of energy absorbed. The light quanta emitted by the scintillator are converted back into electrons by a photocathode. These electrons are subsequently multiplied into electric signals by photomultipliers. The simplified structure of a typical photomultiplier (PM) tube is illustrated in fig.13. The scintillation light after reflection at the inside walls (which are light-tight) enclosing the scintillators fall on the photocathode of the PM tube which is optically coupled to the scintillator. The photoelectrons are emitted from the photocathode and are directed toward the first dynode of the photomultiplier (fig.13), whose potential is about 100V positive with respect to the photocathode. Each electron that strikes the dynodes causes several other electrons to be ejected from the dynode, thereby 'multiplying' the original photocurrent. This

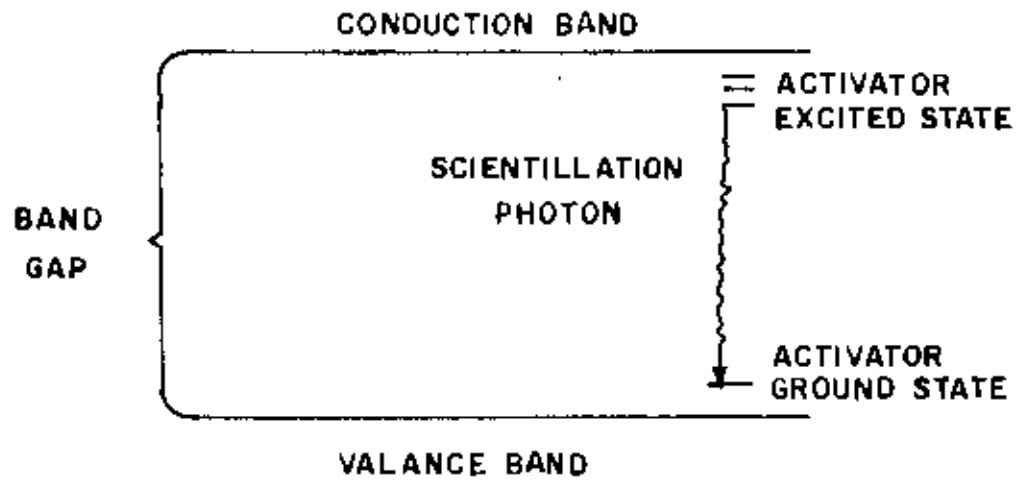


FIG. 11. ENERGY BAND STRUCTURE OF ACTIVATED CRYSTALLINE SCINTILLATOR.

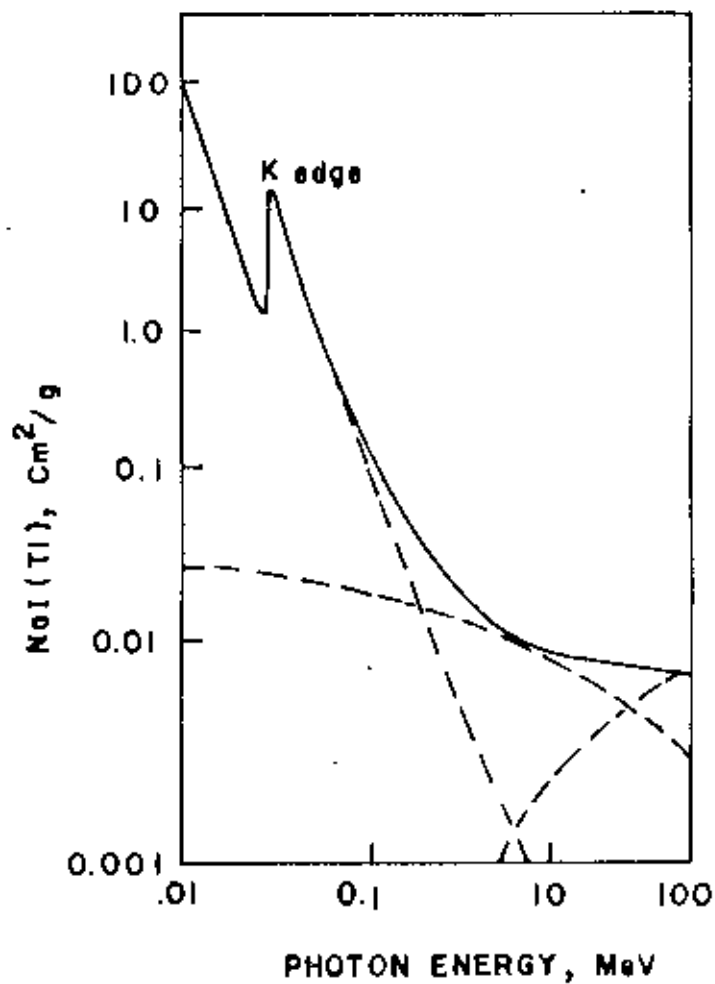


FIG. 12. ENERGY DEPENDENCE OF THE VARIOUS GAMMA RAY INTERACTION PROCESSES IN SODIUM IODIDE CRYSTAL.

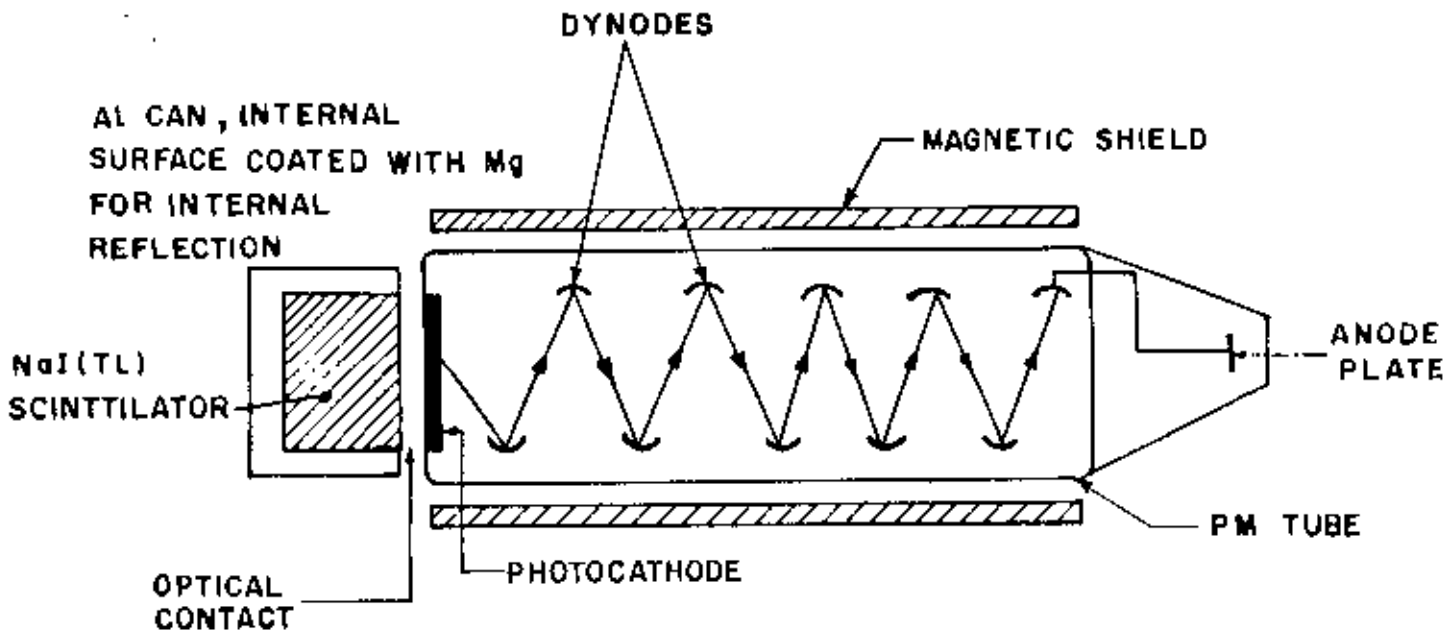


FIG. 13 A SCHEMATIC DIAGRAM OF NaI - PM TUBE SYSTEM.

process is repeated about 10 times before all the electrons, thus produced, are collected by the plate of the PM tube. The resulting current pulses, whose magnitude is proportional to the energy of the primary ionizing radiation, produces voltage pulses at the output of the photomultiplier. The voltage pulses can then be amplified and analysed for counting through conventional circuits (fig.7).

The Model 802 scintillator detector, which is monoline crystal assembly including a high resolution NaI(Tl) crystal and a photomultiplier tube was selected in our experiment to detect gamma-ray photons. Its salient features are shown in Table-6.

Table-6
Specifications of NaI(Tl) detector

Dimension	:	7.6 cm x 7.6 cm
Window	:	0.05 mm aluminium (density: 147.9 mg/cm ³)
Reflector oxide	:	16 mm thick (density 88 mg/cm ³)
Magnetic/light shield	:	connecting lined steel
Bias	:	1000 V
Resolution	:	7.5% at 662 keV peak of ¹³⁷ Cs

5.4 RADIATION SOURCE

The experiment was carried out using a ^{252}Cf fission source which emits both fission neutrons and fission gamma-rays. The total mass was 2 μg on November, 1985, which corresponds to 2.3×10^6 n/sec/ μg and 1.3×10^7 γ / μg . This source was taken because of its fission yield being identical to the fission yield of ^{235}U which undergoes nuclear fission with thermal neutrons in a reactor core⁽³⁶⁾. A typical fission yield distribution for both ^{252}Cf and ^{235}U is shown in figure 14. The average neutron energy of the fission spectrum due to ^{252}Cf and ^{235}U have a mean values of 2.3 MeV and 2 MeV, respectively. Typical neutron and gamma-ray fission spectrum of ^{252}Cf are shown in figures 15a and 15b. Some physical properties⁽⁴⁰⁾ of ^{252}Cf are summarized in Table-7.

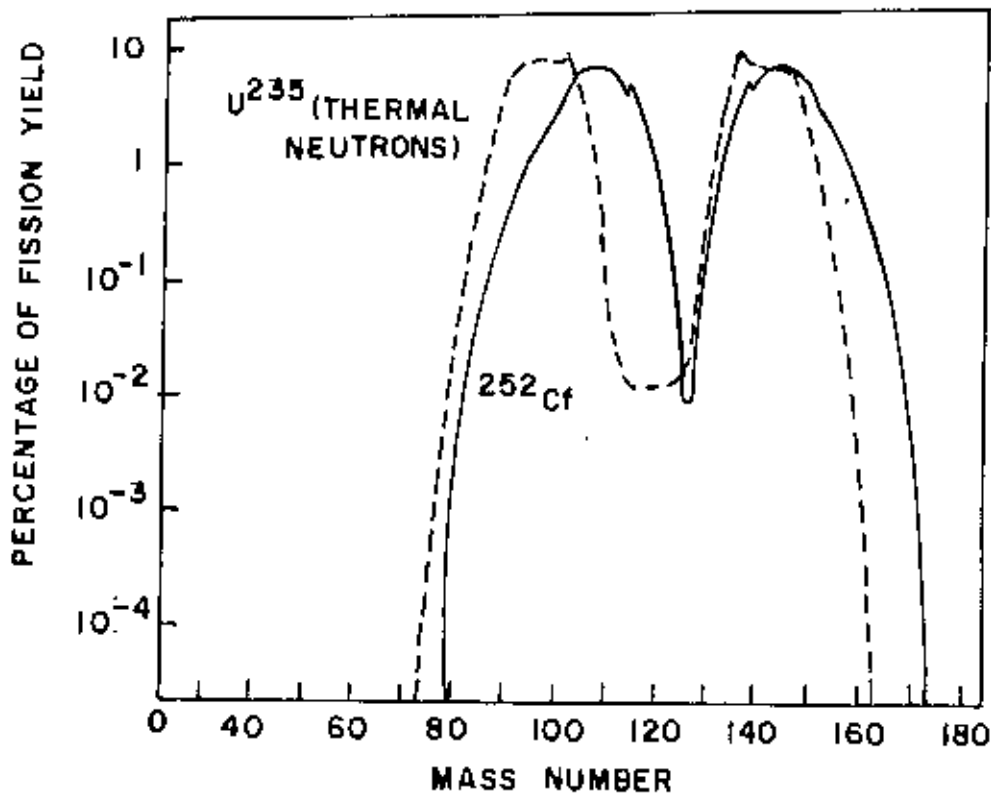
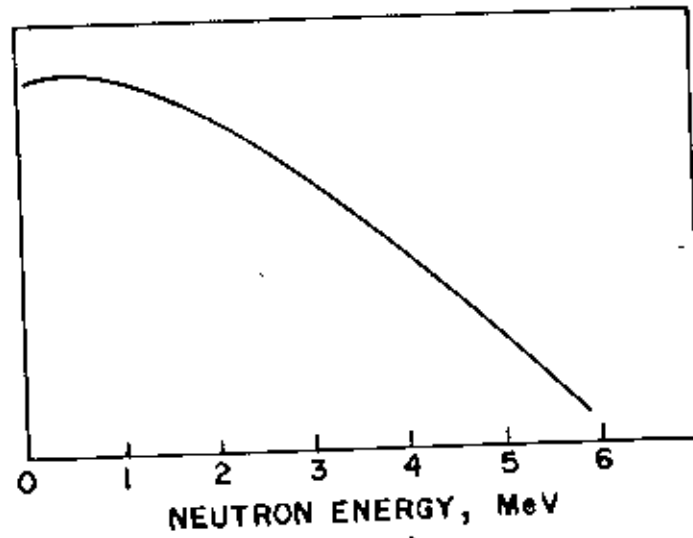
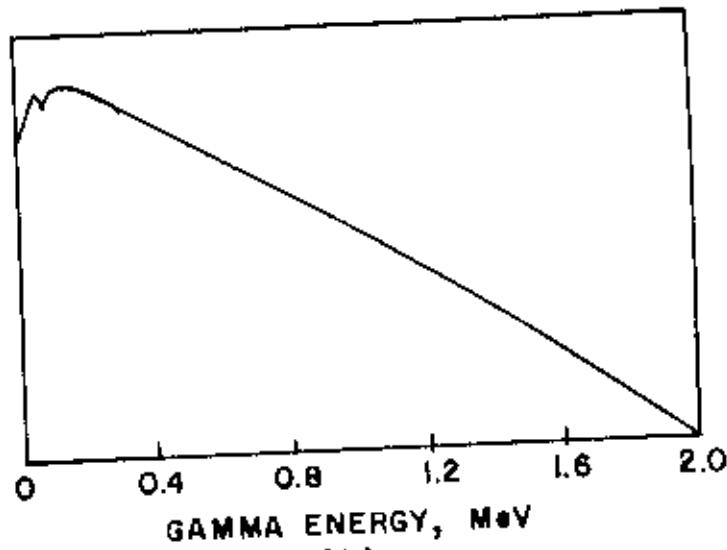


FIG. 14. THE MASS DISTRIBUTION OF ^{252}Cf SPOSTANEOUS FISSION FRAGMENTS AND THE CORRESPONDING DISTRIBUTION FISSION OF ^{235}U INDUCED BY THERMAL NEUTRONS IN A NUCLEAR REACTOR.

RELATIVE NO. OF NEUTRONS



(a)

RELATIVE NO. OF
GAMMA RAYS.

(b)

FIG. 15 (a) NEUTRON ENERGY SPECTRUM OF ^{252}Cf AND
(b) GAMMA ENERGY SPECTRUM OF ^{252}Cf .

Table-7
Physical properties of ^{252}Cf

Atomic number	98
Atomic weight	252
Half-life for alpha emission	2.72 years
Half-life for spontaneous fission	85.5 years
Half-life (effective)	2.65 years
Fraction of decay by alpha emission	97%
Fraction of decay by spontaneous fission	3%
Average number of neutrons per spontaneous fission	3.8
Decay heat (5% from fission, 49% from decay)	39 $\mu\text{W}/\mu\text{g}$
Specific activity	530 $\mu\text{Ci}/\mu\text{g}$
Neutron emission rate	$2.3 \times 10^8 \text{ s}^{-1} \cdot \mu\text{g}^{-1}$
Neutron spectrum	See fig. 6a 5a
Photon emission rate	$1.3 \times 10^7 \text{ s}^{-1} \cdot \mu\text{g}^{-1}$
Gamma radiation spectrum	See fig. 6b 5b

5.5 SHIELDING MATERIALS

The reduction of radiation intensities is accomplished through interaction of radiation with matter. The most significant radiations for which shielding is required are (i) the mixed radiation field consisting of the primary gamma-rays and neutrons present inside a research reactor, neutron generator and also emitted by certain radioactive sources and (ii) the secondary gamma-rays produced by inelastic scattering of fast neutrons with shielding materials and the capture of thermal neutrons. The shield design involves more than choosing a suitable material (or materials) and determining the optimum thickness required to decrease the total radiation to an acceptable level. Elements of high atomic number and high density are the best for absorbing gamma-rays and elements of low atomic number are the best for absorbing neutrons. Heavy elements may be used also to slow down high-energy neutrons by inelastic scattering. Hydrogenous materials i.e., materials containing hydrogen may be used to moderate intermediate neutrons. Neutron poisons, such as boron, may be used to absorb low energy neutrons without emitting high energy gamma-ray. In addition to possessing good attenuation properties, an ideal shielding material should have the following characteristics⁽⁴¹⁾:

- be inexpensive;
- easy to handle and fabricate;
- physically strong and durable under operating conditions;
- stable in chemical composition and physical dimensions;

- fire-resistant;
- noncorrosive, nontoxic, and odorless;
- not affected by intense radiation fields or high temperatures; and
- co-efficient of expansion that is compatible with other materials.

Since no material could have all these qualities, compromises in design and fabrication of mixed radiation shields are required. A brief description of the shield materials used in the multilayer shielding experiments and their properties is presented below:

POLYBORON

It is well known that neutrons are most effectively moderated by hydrogenous materials. Addition of boron in hydrogenous material provides good absorption of neutrons and reduces secondary gamma radiation which is desirable for neutron shielding. A neutron shielding material, called "Polyboron", consisting of polyethylene, boron-ester and paraffin wax⁽⁴²⁾ has been locally developed. The density of this material is little lower than water (0.971 g/cc). Polyboron has unique mechanical properties. The neutron shielding effectiveness of this material has been studied and reported by Bhuiyan et al.⁽⁴³⁾ The polyboron can be used in encapsulated form in locations where the temperature is higher than that of its melting point. It may be used in some other mixed fields of neutrons and gamma-rays like neutron radiography, cancer therapy using reactor neutron beam etc.

CONCRETE

Concrete, one of the most familiar construction materials, has many properties desirable from a nuclear radiation shielding point of view. It is an inexpensive, easily handled material. Its good nuclear properties taken in conjunction with its excellent structural properties. It is a mixture of hydrogen and other light nuclei and nuclei of fairly high atomic number. For these reasons, it is efficient, both in absorbing gamma-rays and slowing down of fast neutrons by elastic and inelastic scattering. The hydrogen contained in the water of hydration of the cement is sufficient for the rapid thermalization of the intermediate energy neutrons. The standard composition of ordinary concrete with a conventional method of preparation is 1 part cement : 2 parts sand : 4 parts rock aggregate by volume and adding about 6 gallons of water per 94lb bag of cement (53 litres water per 100 kg cement). Increasing the cement content will tend to increase the strength of concrete, while increasing the water content will tend to decrease its strength. Special aggregates can be used to increase the density and shielding efficiency. For heavy concrete the desirable water-cement ratio may be less than 0.53.

The ordinary concrete slabs were made with cement, sand and stone chips mixed together in the ratio of 1 : 2 : 3 respectively by volume and the density of ordinary concrete is 2.3 g/cm^3 with compressive strength of 315 kg/cm^2 . The dimensions of each of the slabs is 25.5 cm x 12.5 cm x 5 cm.

The ilmenite-magnetite concrete is a heavy concrete produced with ilmenite, magnetite and ordinary sand together with stone chips and cement. This material has been used as a biological shield of the 3 MW TRIGA Mark-II research reactor at Atomic Energy Research Establishment (AERE), Savar. The heavy concrete is made of ilmenite, magnetite and ordinary (Sylhet) sand mixed together in the ratio 2:2:1 with cement and stone chips in the ratio 100:36:100 by volume. The density of the heavy concrete is 2.75 g/cm^3 with compressive strength of 238.01 kg/cm^2 . These slabs, each having the dimension of 25.5 cm x 12.5 cm x 5 cm, were also supplied by the INST of the AERE, Savar.

LEAD

Because of its high density, good working qualities, lack of objectionable impurities, ability to withstand radiation without damage, and availability in large quantities, lead is a valuable gamma-ray shield. It is particularly effective against low energy gamma-rays because of high photoelectric absorption cross-section which predominates upto gamma-ray energies as high as 0.5 MeV, and also against high energy gamma-rays because of its high pair-production cross-section.

Lead is widely used in the form of rectangular "lead bricks". Because of high density of lead, the volume required for a shield is low, resulting in a comparatively smaller shield. This makes it attractive for shielding mobile reactors and isotope carriers, and for

special application in which it is imperative to reduce materially the size and weight of the shield. Lead is also corrosion resistant and easily fabricable.

It has poor structural properties. As a result large lead sheets and plates must be supported. It is comparatively expensive.

CHAPTER - 6

RESULTS AND DISCUSSION

The relative variation of neutron transmission factor, $I/I(0)$, as a function of thickness for polyboron (PB) + heavy concrete (HC), PB + ordinary concrete (OC) and PB + lead (Pb) multilayer shielding arrangements are plotted in figure 16. It is seen that the PB+HC arrangement shows more attenuation of neutron than those of PB+OC and PB+Pb shielding arrangements. For the thickness of 7.5 cm, the attenuation of neutron observed is 54% for PB+HC shielding arrangement but is 52.5% and 37% for PB+OC and PB+Pb shielding arrangements respectively. For 30 cm thickness, the attenuation of neutron increases to 85.7%, 83.5% and 81.5% for PB+HC, PB+OC and PB+Pb shielding arrangements respectively. The results show that the PB+HC shielding arrangement has greater neutron shielding effectiveness than those of PB+OC and PB+Pb shielding arrangements. The neutron shielding effectiveness of PB+OC is closer to PB+HC but the shielding effectiveness of both these arrangements are higher than that of PB+Pb shielding arrangement. The cause of higher attenuation of neutron in PB+HC arrangement than in PB+OC and PB+Pb shielding arrangements is probably due to the presence of more water molecules in heavy concrete.

The transmission curves for gamma-ray in the same types of multilayer shielding arrangements is shown in figure 17. The curves show that the PB+Pb arrangement contribute more attenuation in gamma-ray transmission than those of PB+HC and PB+OC shielding arrangements.

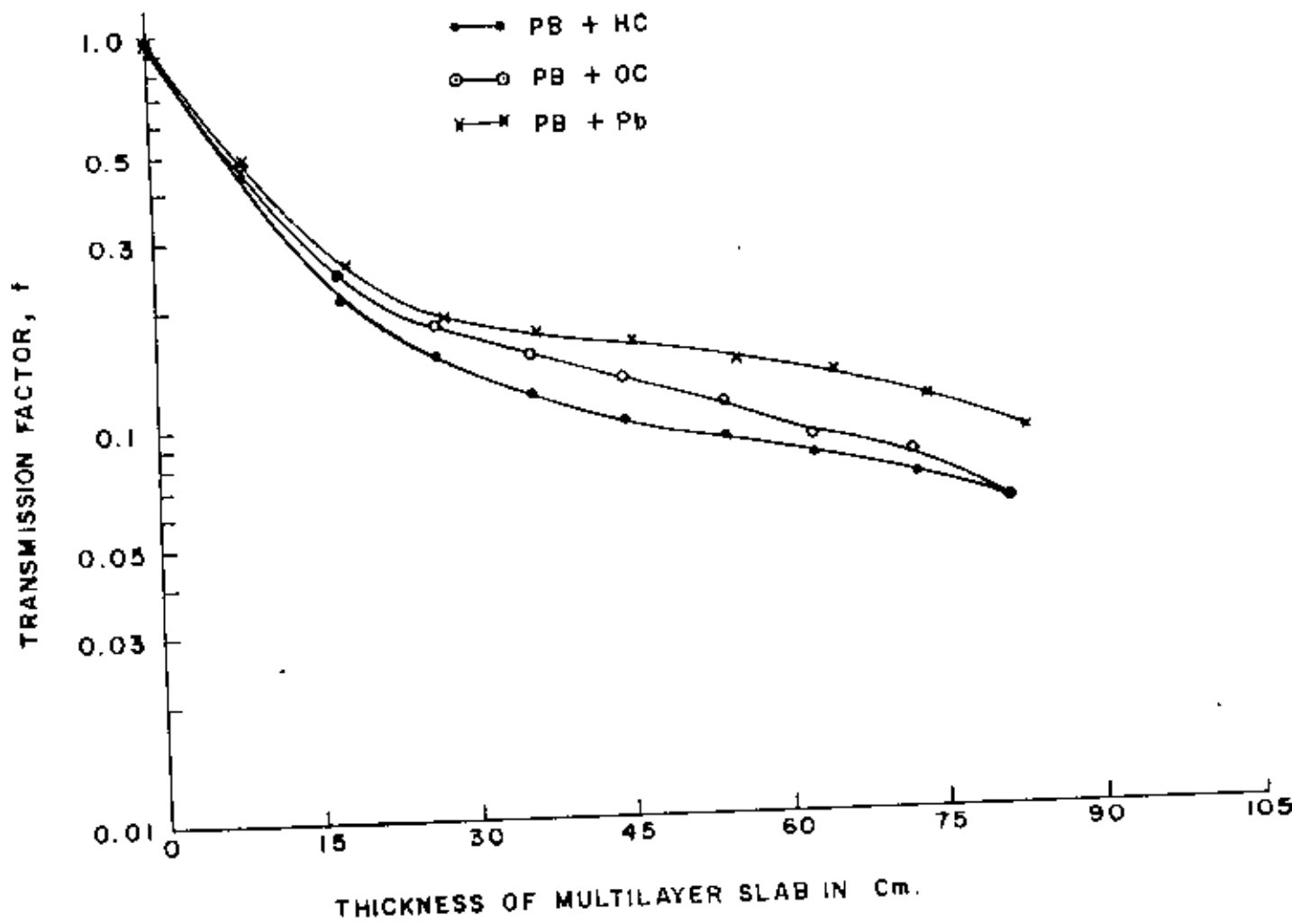


FIG. 16. RELATIVE TRANSMISSION FACTOR AS A FUNCTION OF THICKNESS IN cm FOR PB + HC, PB + OC AND PB + Pb MULTILAYER SHIELDING ARRANGEMENT FOR NEUTRONS.

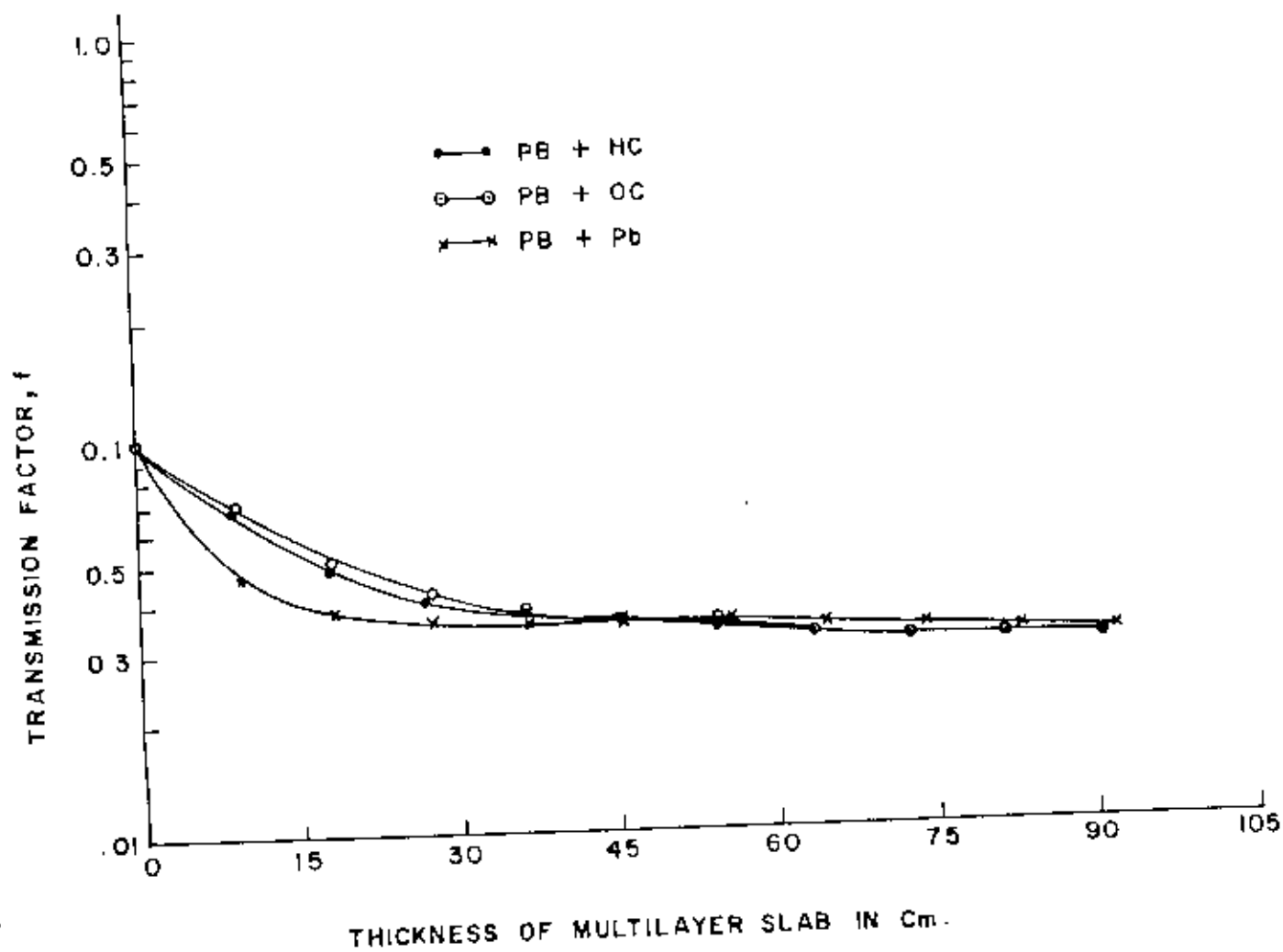


FIG. 17 RELATIVE TRANSMISSION FACTOR AS A FUNCTION OF THICKNESS IN cm FOR PB + HC, PB + OC AND PB + Pb MULTILAYER ARRANGEMENT FOR GAMMA RAYS.

For the thickness of 7.5 cm, the attenuation of gamma-ray intensity observed is 50% for PB+Pb shielding arrangement compared to 28% and 27.4% for PB+HC and PB+OC shielding arrangements, respectively. For 30 cm thickness, the attenuation increases to 66%, 62% and 59%, respectively. The results show that the PB+Pb shielding arrangement has greater gamma-ray shielding effectiveness than those of PB+HC and PB+OC shielding arrangements. The gamma-ray shielding effectiveness of PB+HC is higher than that of PB+OC shielding arrangement but the shielding effectiveness of PB+Pb is more than those of PB+HC and PB+OC shielding arrangements. The higher gamma-ray attenuation in PB+Pb shielding arrangement than in PB+HC and PB+OC arrangements is probably due to the higher density of the lead.

The relative rate of counts for neutron and gamma-ray as a function of thickness of multilayer slabs are shown in figures 18 and 19. The attenuation of neutron and gamma-ray intensity is generally characterized by half-value thickness (HVT), removal cross-section (Σ_R), attenuation co-efficient (μ) and relaxation length (λ). The attenuation characteristics based on the measured values from the attenuation curves for neutron and gamma-ray are given in Tables 8 and 9. The values presented in these tables are deduced from the slopes of the curves (Figures 18 and 19). Since the relaxation length of a particular radiation in a given material is equivalent to the reciprocal of the attenuation co-efficient (for gamma-ray) or removal cross-section (for neutron), the relaxation lengths provide a good means for comparing the

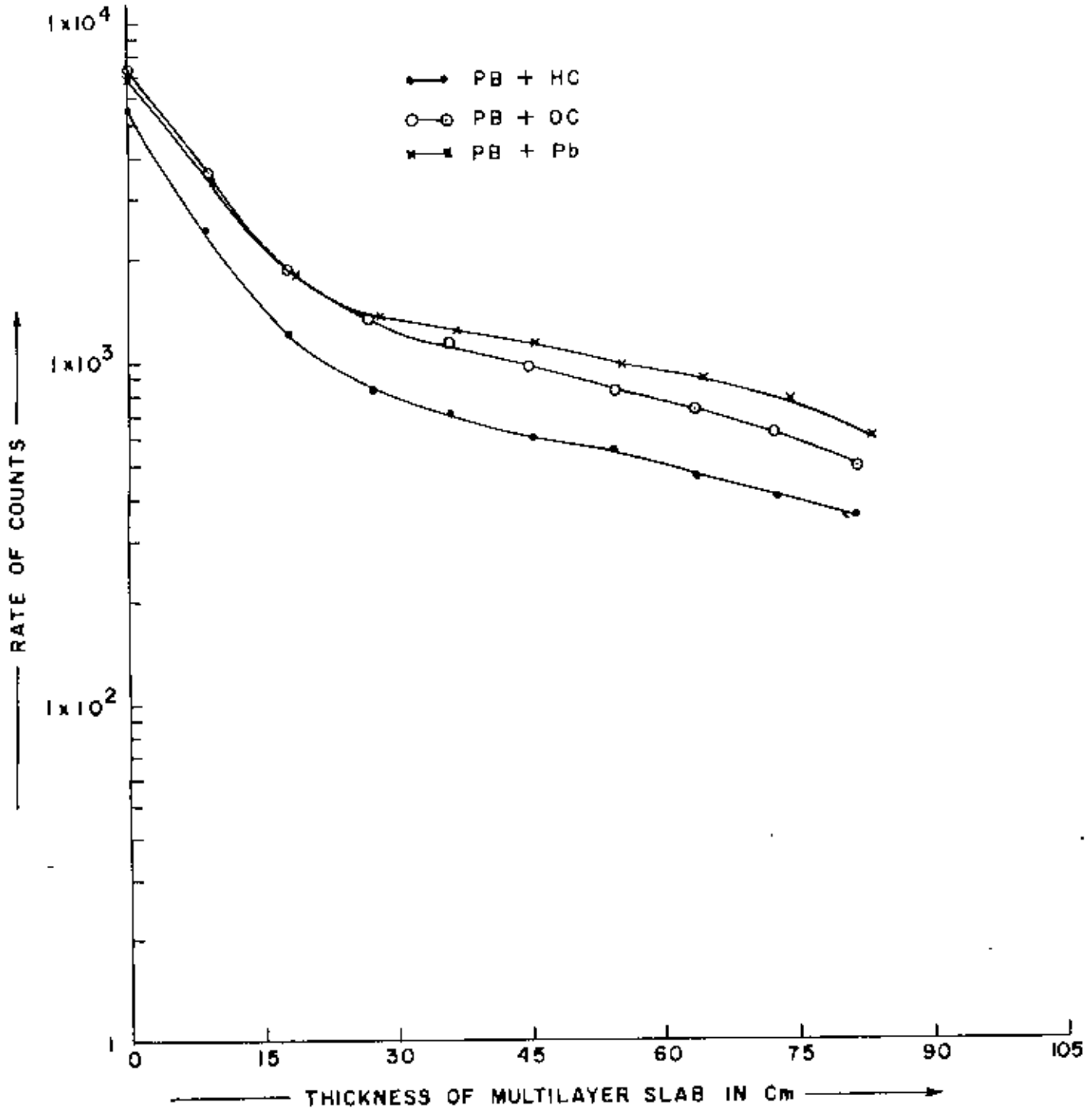


FIG. 18. RELATIVE RATE OF COUNTS AS A FUNCTION OF THICKNESS IN cm FOR PB + HC, PB + OC AND PB + Pb MULTILAYER SHIELDING ARRANGEMENT FOR NEUTRONS.

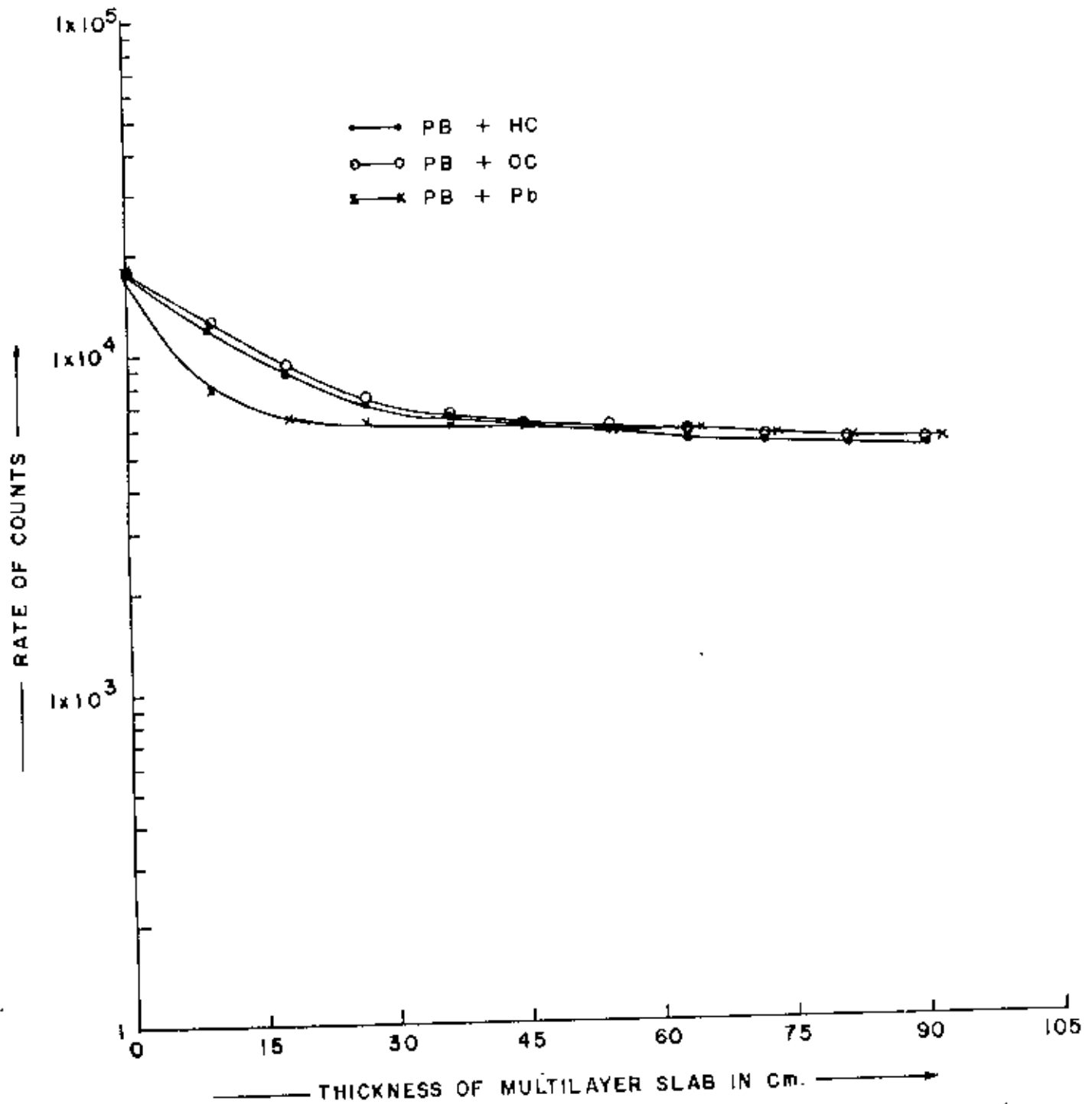


FIG. 19. RELATIVE RATE OF COUNTS AS A FUNCTION OF THICKNESS IN cm
PB + HC, PB + OC AND PB + Pb MULTILAYER SHIELDING
ARRANGEMENT FOR GAMMA RAYS.

shielding effectiveness of different multilayer materials.

Table-8 shows that the relaxation length for neutron in PB+HC is much smaller than the relaxation lengths in PB+OC and PB+Pb shielding arrangement. This is because the HC may has more hydrogen content than the OC and Pb is a heavy element of poor neutron attenuation capacity.

Table-9 shows that the relaxation length for gamma-ray in PB+Pb shielding arrangement is much smaller than those of PB+HC and PB+OC shielding arrangements. Lead has very high density and large absorption coefficient for gamma-ray resulting in good attenuation capacity for gamma-rays.

A comparison of the present measurement of neutron and gamma-ray attenuation characteristic (Tables 8 and 9) with those obtained in other investigations cannot be made directly because different composition and constituents of the concretes and lead have been used^(45,46). Furthermore, data on the attenuation of the radiation from ^{252}Cf for concretes is not available. However, for comparison, the available data on relaxation length for neutron in different concretes and lead are shown in Table-10. The relaxation lengths for neutron obtained in this study are generally comparable with published value (Table-10), being slightly better for few cases. The shielding performance depends on the properties of component substances; and by suitable choice of constituents it is possible to increase the density of material and optimize the shielding characteristics for various types of radiation.

The locally available ilmenite and magnetite sand have great economical potential for use in the development of high density (heavy) concrete for effective shielding of neutron attenuation in a nuclear radiation field.

Table-8

Nuclear parameters by neutrons in multilayerd shields.

Combination of multilayerd shields	Half-value thickness (cm)	Tenth-value thickness (cm)	Removal cross-section Σ_R , (cm^{-1})	Relaxation length (cm)
PB+HC	6.5	57.0	0.1066	9.38
PB+OC	8.25	66.5	0.0840	11.90
PB+Pb	9.0	76.5	0.0770	12.99

Table-9

Nuclear parameters by gamma-rays in multilayerd shields

Combination of multilayerd shields	Half-value thickness (cm)	TVT (cm)	Attenuation coefficient, μ (cm^{-1})	Relaxation length (cm)
PB+HC	17.25	-	0.0402	24.89
PB+OC	18.60	-	0.0372	26.84
PB+Pb	8.0	-	0.0866	11.54

Table-10

Typical values of the relaxation lengths neutron in concretes (Ref.1) and lead (Ref.2).

Type of shielding material	Density (g/cm ³)	Relaxation length (cm)
Ordinary Concrete	2.30	12.2
Ilmenite	3.52	13.4
Concrete		
Magnetite	3.29	8.9
Concrete	3.50	10.5
Limonite	2.70	9.0
Lead	11.3	9

CHAPTER -7

CONCLUSION

Thermal neutron flux at different distances from the biological shielding face of the research reactor in the tangential beam port have been measured by activation method. Gold foils of high purity have been irradiated in the central beam axis of the beam port. Measured neutron flux has been found to decrease as the distance increases from the biological shielding face of the reactor. Neutron flux was found to be maximum (4.34×10^7 n/cm²/sec) near the biological shielding face and minimum (1.08×10^7 n/cm²/sec) at a distance of 1.5 m away from the same face.

The results of the present investigation on the effectiveness of multilayered shields for gamma rays suggest that a multilayered shield of polyboron-lead is more effective than those of polyboron-heavy concrete and polyboron-ordinary concrete. This is explained by the fact that attenuation of gamma-rays in polyboron-lead is higher than those of polyboron-heavy concrete and polyboron-ordinary concrete.

The results of the present investigation on the effectiveness of multilayered shield for neutrons suggest that a multilayered shield polyboron-heavy concrete is more effective than those of polyboron-ordinary concrete and polyboron-lead. This is due to the fact that attenuation of neutrons in polyboron-heavy concrete is more than those of polyboron-ordinary concrete and polyboron-lead.

Finally, it is concluded that a multilayered shield consisting of polyboron, heavy concrete and lead may find its useful applications in a mixed field of neutrons and gammas such as in beam port experiments in research reactors, accelerators and neutron generators and also in the uses of radioisotopic neutron sources.

REFERENCES

1. CANBERRA, Instruments for use preamplifier, amplifier of semi-conductor detector.
2. N. Stroken, V. Ajdacic, and D. Lalovic, Nucl. Instr. and Meth., 94, 147, 1971.
3. CANBERRA, Germanium detector, operating manual.
4. 0-5 KV, H.V. POWER SUPPLY MODEL 3105 Operator's manual.
5. CANBERRA, Preamplifier Operating Manual.
6. Instruction Manual of 4096 Multichannel Analyzer.
7. R.G. Helmer, Precise efficiency calibration of Ge semi-conductor detectors for 50-2000 KeV gamma-ray.
8. M. Rahman, N.I. Molla, A.A.Z. Ahmad, Proc. Seminar on Operation and Utilization of Research Reactor at AERE, Savar, Dhaka, Sept. 14, 1987, page-78.

M. Rahman, Rebazuddin Miah, Ayesha A. Khan, A.A.Z. Ahmad and M.A. Rahman, Proc. of the 2nd seminar on Operation and Utilization of the Research Reactor at AERE, Savar, Dhaka, February, 1989, page-91.
9. A.S. Makarious, M.A. El-Kolaly, I.I. Bashter and W.A. Kansouh, Appl. Radiat. Isot., 40, 257, 1989.
10. Kchitaro Ueki and Yoshihito Namito, Nucl. Sci. and Engg., 96, 30, 1987.

11. R.M. Megahid et al, *Int. J. Appl. radiat. and Isot.*, 36, 307, 1985.
12. T. Maruyama et al, *Health Physics*, 20, 277, 1971.
13. G.D. Bishop, *Ann. Nucl. Energy*, 9, 233, 1982.
14. Yoshiaki Oka, Shigehiro An, and Shigeru Kasai, *Nucl. Sci. Engg.*, 73, 259, 1980.
15. S.C. Gujrathi and J.M. D'Auria, *Nucl. Instr. and Meth.*, 100, 445, 1972.
16. Y. Uwamino et al, *Nucl. Sci. Engg.*, 80, 360, 1980.
17. F.E. Senffle and P. Philbin, *Health Phys.*, 23, 532, 1972.
18. R.J. Adams and K.H. Lakan, *Proc. Conf. on nuclear cross sections*, NBS special publication 425, Vol.1, 409, 1975.
19. R.J. Adams and K.H. Lakan, *Health Phys.*, 36, 671, 1979.
20. S. Makra et al, *Kerenergic*, 16, 378, 1973.
21. F.U. Ahmed et al, *Measurement of gamma-ray shielding properties of I-M Concrete and Poly-boron slabs using Cf-252*. Submitted for publication in *Nucl. Sci. Engg.*
22. S.I. Bhuiyan et al, *Health Phys.*, 57, 1989.
23. F.U. Ahmed et al, *Nucl. Sci. Engg.*, 85, 427, 1983.
24. P.T. Robson et al, *Sov. At. Energy*, 32, 241, 1976.
25. P.H. McGinley, *Health Physics*, 23, (July), 105, 1972.

26. A.O. Hanson and M.L. McKibben, *Phys. Rev.*, 72, 673, 1947.
27. M.H. McTaggart, *AWRE NR/AI/59*, 1958.
28. L.V. East and R.B. Walton, *Nucl. Instr. and Meth.*, 75, 231, 1969.
29. G.F. Knoll, *Radiation Detection and measurement*, John Willey and Sons, Inc., USA, 1972.
30. J.W. Leake, *Nucl. Instr. and Meth.*, 63, 329, 1968.
31. H.E. Thies and K.J. Botcher, *Nucl. Instr. and Meth.*, 75, 231, 1969.
32. J. De Pangher and L.L. Nichols, *BNWL-260*, 1966.
33. L.V. East et al, *Nucl. Instr. and Meth.*, 72, 161, 1969.
Gamma-ray detector.
34. H. Cember, *Introduction to Health Physics, Second Edition*, Pergamon Press, UK, 1985.
35. B.T. Price, C.C. Horton and K.T. Spinney, *Radiation Shielding*, Pergamon Press, UK, 1957.
36. H. Goldstein, *Fundamental aspects of Radiation Shielding*, Pergamon Press, UK, 1956.
37. S. Glasstone and A. Sesonske, *Nuclear Reactor Engineering*, Van Nostrand Co., Princeton, V.J., 1967.
38. Hofstadter, R., and J.A. McIntyre; *Phys. Rev.* 74, 100, 1948.
39. G.J. Hiline, *J. Nucl. Med.*, 18, 867, 1977.
40. *International Atomic Energy Agency Technical Reports Series*
No. 159, Vienna, 1974.

41. McLain Martens, Reactor hand book engineering, Vol. IV.
42. M. Ahsan, S.I. Bhuiyan, F. Akhter, M.A. Rouf and S.R. Husain, INST-10, AERE, Dhaka, P.O. Box 3787, 1984.
43. S.I. Bhuiyan, F.U. Ahmed, A.S. Mollah, and M.A. Rahman, Studies of the neutron transport and shielding properties of locally developed shielding material: Polyboron, Health Phys. Vol. 57, (1989) (in press).
44. J.P. Kuspa and N. Tsoulfanidis, Nucl. Sci. Engg., 52, 117, 1973.
45. H.E. Hungerford et al, Engineering Compendium on Radiation Shielding, vol.II, Shielding Materials (R.G. Jeager, Ed. in Chief), sec., 9.1.12, 1975.
46. Nuclear Engineering Hand Book, Harold Etherington, McGraw Hill Book Company. Sec. 8.3, 1958.

